Report Number
TM-62-3

Calculations of Flow Characteristics for Two-Phase Flow in Annular Converging-Diverging Nozzles

by

D. W. Netzer

Contract N-onr-2160(21)

June 1962

JET PROPULSION CENTER
PURDUE UNIVERSITY
SCHOOL OF MECHANICAL ENGINEERING
LAFAYETTE, INDIANA

PURDUE UNIVERSITY

AND

PURDUE RESEARCH FOUNDATION
Lafayette, Indiana

Report No. TM-62-3

Technical Memorandum

CALCULATION OF FLOW CHARACTERISTICS FOR TWO-PHASE FLOW IN ANNULAR CONVERGING-DIVERGING NOZZLES

D. W. Metzer

Approved by: M. J. Zucrow

M.J. Zucrow
Atkins Professor of
Engineering

Contract N onr 1100(21)

Jet Propulsion Center
Purdue University

June 1962

ACKNOWLEDGMENTS

Appreciation is expressed to Dr. N. J. Zucrow, Atkins Professor of Engineering and to Dr. C. F. Warner, Professor of Mechanical Engineering for their guidance and assistance during the course of this research.

Appreciation is also expressed to Mr. David L. Reid for his help in performing the experimental phase of the investigation, to Mr. Harold M. Cassaday for his help in performing the experimental work and data reduction, and to Mr. Stuart D. Kershner for his help with the computer progaming.

Acknowledgment is also given to the Office of Naval Research, Contract Number 1100(21), under whose sponsorship the research reported herein was conducted. Reproduction in full or in part is permitted for any use of the United States Government.

TABLE OF CONTENTS

LIST OF TABLES

LIST OF ILLUSTRATIONS

ABSTRACT

This report presents an analytical method for determining the flow characteristics of a two-phase flow of liquid drops in a gas stream as the mixture expands through an annular converging-diverging nozzle. The subject analysis can be utilized to predict the liquid velocity, gas velocity, static pressure, and droplet diameter as a function of axial distance along the nozzle for a two-phase flow that contains approximately ten times as much liquid as gas by weight.

The analysis was programmed for solution on an RPC 4000 Digital Computer. Two nozzle configurations were investigated. Both nozzles had the same converging angle of 20°, throat radius of one inch, inlet area of 3.287 $in.^2$, throat area of 0.267 $in.^2$ and exit area of 2.450 $in.^2$. One nozzle had a total diverging angle of 7° and the other had a total diverging angle of 21°.

The liquid and gas utilized in this investigation were water and air respectively. Flow rates of between 8 and 11 lb/sec of water and between 1.0 and 1.3 lb/sec of air were utilized. The liquid and gas were expanded from a low velocity and a pressure of 500 psig to ambient pressure. Predicted exit velocities ranged between 700 and 900 ft/sec

for the air and between 600 and 800 ft/sec for the water.

Droplet break-up (or critical decomposition) was considered in the subject analysis. An assumed initial droplet diameter of 0.020 inches decreased in size to between 0.0008 and 0.0010 inches at the nozzle exit. The Weber number governs droplet break-up and a critical Weber number of 6.3 was employed herein.

Experimental work was performed in order to check the theoretically predicted pressure profiles, flow rates of liquid and gas, and the thrust. The theoretical and experimental pressure profiles matched quite closely for both nozzles investigated. When the gas flow rate was one-tenth that of the liquid flow rate by weight, the pressure profiles matched more closely than when the gas flow rate was 0.15 that of the liquid flow rate. The predicted total flow rates were within four to nine percent of those obtained experimentally.

The thrust was predicted to an accuracy of approximately three percent for the short nozzle, but to an accuracy of only approximately twenty percent for the long nozzle.

From the investigation it was concluded that the subject analysis can be utilized to predict the flow characteristics of a two-phase flow of liquid drops in a gas stream for relatively short nozzles with the flow rate of liquid approximately ten times the flow rate of gas by weight.

1 INTRODUCTION

The analytical method developed herein can be employed to determine the following flow characteristics of a two-phase flow of liquid drops in a gas stream as the mixture expands through a converging-diverging nozzle: gas velocity, droplet velocity, static pressure, and droplet size. This work was initiated in conjunction with an investigation of the operating characteristics of a gas-driven jet pump (1) (2)*. The drive nozzle for such a device operates with a typically low mixture ratio.** Previous investigations at the Jet Propulsion Center, Purdue University (1,2) have shown that an operating mixture ratio of approximately 0.10 should be utilized for optimum jet pump operation. At low mixture ratios a larger quantity of liquid is pumped for a given flow rate of gas than at high mixture ratios.

A two-phase nozzle is a device through which two fluids are accelerated from low velocities and a high pressure to high velocities and a low pressure. In the subject analysis water and air are the two fluids. The two fluids are injected into the nozzle from an injector which is designed to break the water up into droplets and distribute them evenly

---

* Numbers in parenthesis refer to references appearing in the rear of the report.

** Mixture Ratio - defined as the mass flow rate of gas ($\dot{W}_G$) over the mass flow rate of liquid ($\dot{W}_L$) - or $\dot{W}_G/\dot{W}_L$

in the air. When the two fluids enter the converging portion of the nozzle the gas expands, and therefore its velocity increases more rapidly than the liquid. The liquid droplets accelerate as a result of (1) the decreasing pressure in the direction of flow and (2) the drag forces exerted on them by the faster moving gas.

The droplets will undergo critical decomposition* if the inertial forces exerted on them exceed the surface tension forces. This phenomenon is governed by the Weber number. The Weber number is defined as follows:

$$N_{We} = \frac{\rho_G V_R^2 r}{\sigma} \qquad (1)$$

where

ρ_G = gas density

V_R^2 = square of the relative velocity between gas and liquid

r = droplet radius

σ = surface tension

The critical Weber number** for water droplets in air is approximately 6.3. This average value of the critical Weber number was determined experimentally by Isshiki for water droplets with diameters from 0.0181 in. to 0.1924 in.(3). The initial drop diameter assumed in this analysis was 0.02 in. and the final diameter ranged between 0.0008 in. and 0.0010 in.

---

* Critical Decomposition - Breaking up of droplets into smaller droplets.

** Weber number at which critical decomposition will occur.

Isshiki's work indicated that the critical Weber number did not vary greatly with droplet size. No other data could be found for smaller droplets and therefore, the average value of 6.3 determined by Isshiki was utilized.

During the expansion of the two-phase mixture through the nozzle, thermal energy is transferred between the liquid and the gas. In the subject investigation, the water is assumed to give up heat to the expanding air. The amount of heat transferred between the phases in a given period of time depends upon (1) the difference in temperature of the two phases, (2) the amount of heat lost through the nozzle boundaries, (3) the shape and size of the liquid droplets, (4) the velocities of each of the fluids, and (5) the thermal characteristics of the individual phases which includes the heat transfer coefficients and the effects of condensation and vaporization.

There are two limiting cases of the heat transfer between phases (1) perfect thermal equilibrium and (2) no thermal energy transfer. Perfect thermal equilibrium assumes an infinite heat transfer rate between phases such that both of the fluids remain at the same temperature throughout the expansion. No thermal energy transfer assumes that no heat will be transferred between the two fluids. In this case, the temperature of the gas decreases during the expansion following the isentropic relationships governing perfect gas flow through a nozzle. The temperature of the water remains constant at the initial inlet value.

The actual case of heat transfer between the two phases lies somewhere between the two limiting cases. D. G. Elliott and D. L. Crabtree

have treated these cases in detail (1) (2).

There are several causes for the loss in total momentum in a two-phase expansion Some of these are (1) wall friction, (2) droplet decomposition, (3) non-uniform distribution of the droplets in the gas, (4) non-ideal heat transfer between the two phases and (5) the relative velocity (or slip) between phases.

The effects of the above mentioned causes for a loss in total momentum of the mixture have been investigated in previous work at the Jet Propulsion Center, Purdue University (1) (2) (4).

2 THEORETICAL ANALYSIS

2-1 Purpose of Analysis

The subject analysis of a two-phase expansion of liquid drops in a gas stream flowing through a converging-diverging nozzle is made in order that the droplet velocity, gas velocity, static pressure and droplet diameter may be predicted as functions of axial distance along the nozzle. More specifically, the subject analysis is made in order to determine the above mentioned flow parameters in a mixture containing a much larger amount of liquid than gas by weight (typically $\dot{W}_L = 10\ \dot{W}_G$).

2-2 Assumptions

The following assumptions were employed in this analysis:

1. The two-phase flow is steady and one dimensional.
2. Drag forces exist between the liquid droplets and the gas.
3. There are no losses due to wall friction.
4. The liquid is in the form of droplets with an assumed initial equivalent spherical diameter.
5. Critical decomposition of the droplets (droplet break-up) does occur. The droplets are uniformly distributed in the gas and are of equal size at any cross-section of the nozzle.
6. There is no interaction between droplets.
7. The liquid is incompressible, has a constant specific heat, and has no vapor pressure.

8. The gas is perfect and has constant specific heat at constant pressure and constant volume.
9. No external work is performed.
10. There is no heat transfer across the nozzle boundaries.
11. Potential energy is a constant.
12. The flow is isothermal.

The assumption of isothermal flow requires further explanation. The equations governing the two limiting cases of heat transfer between the phases, which were discussed above, have been derived by D. G. Elliott (1). The following two equations were taken from that work.

Limiting Case I: Thermal equilibrium between phases with no loss in entropy.

Initially, $T_L = T_G = T_N$

After expansion, $T_L = T_G = T_N$

$$\frac{T_L}{T_N} = \frac{T_G}{T_N} = \left(\frac{P}{P_N}\right)^{\frac{(\dot{W}_G/\dot{W}_L)(\bar{R}/JW)}{C_L + C_p(\dot{W}_G/\dot{W}_L)}} \qquad (2)$$

where

T_N = temperature of mixture at inlet to nozzle,

T_L = liquid temperature at any cross section of the nozzle,

T_G = gas temperature at any cross section of the nozzle,

$\dot{W}_G$ = mass flow rate of gas,

$\dot{W}_L$ = mass flow rate of liquid,

$\bar{R}$ = universal gas constant,

W = molecular weight of the gas,

J = mechanical equivalent of heat, 778 ft lb/B,

C_L = specific heat of the liquid,

C_P = specific heat of the gas at constant pressure,

P_N = pressure of the mixture at inlet to nozzle, and

P = pressure at any point downstream of the inlet.

Limiting Case II: No heat transfer between phases and no loss in entropy.

Initially, $T_L = T_G = T_N$

$$T_L = \text{constant}$$

After expansion, $T_G < T_L$, $T_L = T_N$

$$\frac{T_L}{T_N} = 1, \quad \frac{T_G}{T_N} = \left(\frac{P}{P_N}\right)^{\bar{R}/J\, C_P W} \tag{3}$$

The inlet pressure and temperature of the two-phase mixture employed in this investigation were 514.7 psia and 510°R respectively. The drops in temperature which would occur for the two limiting cases are found by substituting P_N = 514.7 psia and T_N = 510°R with the corresponding specific heats and gas constant into equations 2 and 3 above.

For

P = 14.7 psia

P_N = 514.7 psia

$\bar{R}/W$ = 53.3 ft lb/lb R

$$C_L = 1.0 \text{ B/lb R}$$

$$C_P = 0.24 \text{ B/lb R}$$

The results are shown in Table 1.

Table 1

Results of Calculations for Limiting Cases of Heat Transfer Between Phases

Case	$\dot{W}_G/\dot{W}_L$	P (psia)	T_G (R)	T_L (R)	ΔT_G	ΔT_L
I	0.10	14.7	498	498	12	12
I	0.15	14.7	487	487	23	23
II	any value	14.7	184	510	326	

Experimental work performed at the Jet Propulsion Center, Purdue University, has indicated that the real case of heat transfer between phases is closer to that of thermal equilibrium than to that of no heat transfer between phases (1)(2)(4). The thermal equilibrium temperature drop for a mixture ratio of 0.10 is only 12°R. For these reasons the assumption of isothermal flow was made. A so-called "average temperature" was employed throughout this analysis. This "average temperature" is the average between the inlet temperature chosen and the exit temperature of the mixture calculated with the thermal equilibrium equation 2. The thermal equilibrium temperature drop for a mixture ratio of 0.20 is 23°R. It should therefore be expected that the isothermal model will have limited accuracy as the mixture ratio increases in value much above 0.10.

In order to find a more correct drag coefficient for the droplet than that obtained from the plot of Reynolds Number vs. Drag Coefficient for a solid sphere in a gas stream (5), a survey was made of existing literature on the subject of drag on droplets in an air stream. It was decided that the best data to utilize would be that experimentally determined by E. Robin, R. B. Lawhead, and A. R. Schallenmuller at Rocketdyne, and by R. D. Ingebo at the Lewis Flight Propulsion Laboratory (6)(7). The drag coefficient of liquid droplets having diameters from 0.004 in. to 0.04 in. was determined to be approximately one and appeared to be independent of Reynolds number for Reynolds number greater than fifty (6). The Reynolds number referred to throughout this work is the droplet Reynolds number. It is calculated by employing the relative velocity between phases and the droplet diameter in the defining equation for the Reynolds number.* For very small droplets and Reynolds numbers less than fifty, Ingebo's data were in agreement with that obtained at Rocketdyne. Ingebo's equation for the drag coefficient of a small droplet in an air stream is as follows:

$$C_D = \frac{27}{N_R^{0.84}}$$

In the subject analysis the drag coefficient was assumed to be one for Reynolds numbers above fifty. For Reynolds numbers less than fifty, Ingebo's equation for the drag coefficient was employed.

---

* See Section 2-4.5.

2-3 Equations Employed

The following equations and relationships were employed in the subject analysis:

1. a momentum equation for the system,
2. a force balance on the droplet,
3. a continuity equation for the mixture,
4. the equation of state for the gas
5. the drag equation,
6. the defining relationship for Reynolds number
7. the defining relationship for weber number,
8. the relationship of nozzle flow area to axial distance along the nozzle, and
9. the relationship that the total flow area is equal to the sum of the flow areas of gas and liquid at any cross-section.

2-4 Derivation of the Equations Employed in the Analysis

2-4.1 Momentum equation for the system

Consider a small cross-section of the nozzle of width dx shown in Fig. 1. At the left face the gas velocity, liquid velocity, pressure, and area are denoted by V_G, V_L, p, and A_T respectively. At the right face all of the quantities have increased by differential amounts as indicated in Fig. 1.

Summing the forces in the X-direction.

$$\Sigma F_x = pA_T - (p+dp)(A_T+dA_T) + (p+dp/2)\ \sin\alpha\ (dA_T/\sin\alpha)$$

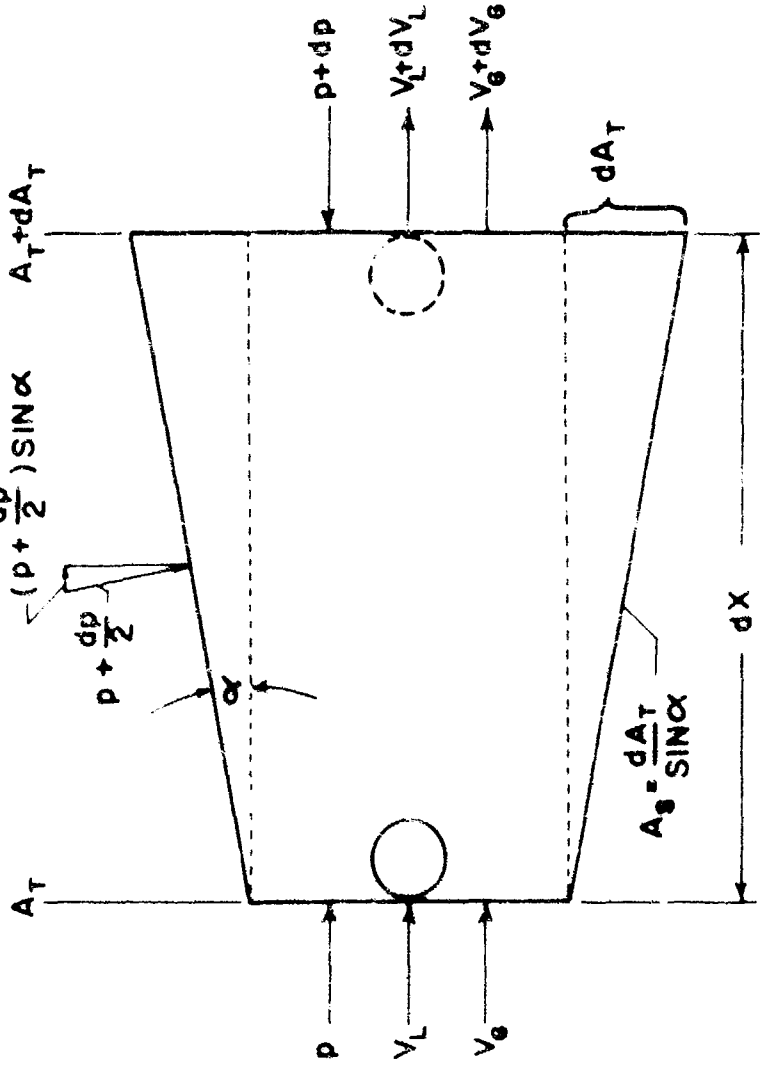

FIG. 1 SMALL SECTION OF A NOZZLE

Multiplying products and neglecting differentials of higher order than one,

$$\Sigma F_x = -\bar{A}_T \, dp \quad *$$

The summation of the forces in the X-direction is equal to the change in momentum of the gas and liquid in that direction.

$$\Sigma F_x = -\bar{A}_T \, dp = \dot{M}_L dV_L + \dot{M}_G dV_G$$

Substituting $\dot{M}_L = \rho_L \bar{A}_L \bar{V}_L$ and $\dot{M}_G = \bar{\rho}_G \bar{A}_G \bar{V}_G$

$$\Sigma F_x = -\bar{A}_T dp = \rho_L \bar{A}_L \bar{V}_L dV_L + \bar{\rho}_G \bar{A}_G \bar{V}_G dV_G \tag{4}$$

where

$\dot{M}_L$ = mass flow rate of liquid,

$\dot{M}_G$ = mass flow rate of gas,

ρ_L = liquid density,

$\bar{\rho}_G$ = average gas density,

$\bar{A}_G$ = average flow area of the gas,

$\bar{A}_L$ = average flow area of the liquid,

$\bar{V}_L$ = average liquid velocity, and

$\bar{V}_G$ = average gas velocity.

$\bar{A}_T$ = average total flow area

Rearranging Equation 4,

$$dp = \frac{\rho_L \bar{A}_L \bar{V}_L dV_L + \bar{\rho}_G \bar{A}_G \bar{V}_G dV_G}{-\bar{A}_T} \tag{5}$$

---

* The bar ($\bar{\ }$) over any quantity indicates the average value of that quantity in any given increment dx.

2-4.2 Force balance on the droplet

Consider a single spherical droplet of liquid traveling in a faster moving expanding gas. Two forces tend to accelerate the droplet; (1) the pressure force resulting from the pressure gradient in the direction of flow, and (2) the drag force exerted on the droplet by the gas. Writing a force balance on the droplet,

$$F_P - F_D = m_d a_d = m_d dV_L/dt = m_d V_L dV_L/dX \qquad (6)$$

where

F_P = force due to pressure,

F_D = force due to drag,

m_d = mass of the droplet,

a_d = acceleration of the droplet, and

V_L = droplet velocity.

The force due to drag is determined by the standard drag equation.

$$F_D = (1/2)\,\bar{\rho}_G \bar{A}_d \bar{V}_R^2 \bar{C}_D \qquad (7)$$

where

$\bar{C}_D$ = average value of the drag coefficient for the increment in question, and

$\bar{A}_d$ = average projected area of the droplet.

The force exerted on the droplet as a result of the pressure variation around it can be determined by considering a small portion of the surface area of the droplet dA as shown in Fig. 2. A pressure force P acts upon this area dA.

The droplet has a radius r. Then, $dA = rd\theta\,(r \sin\theta\, d\phi)$ and $X = r \sin\theta \cos\phi$.

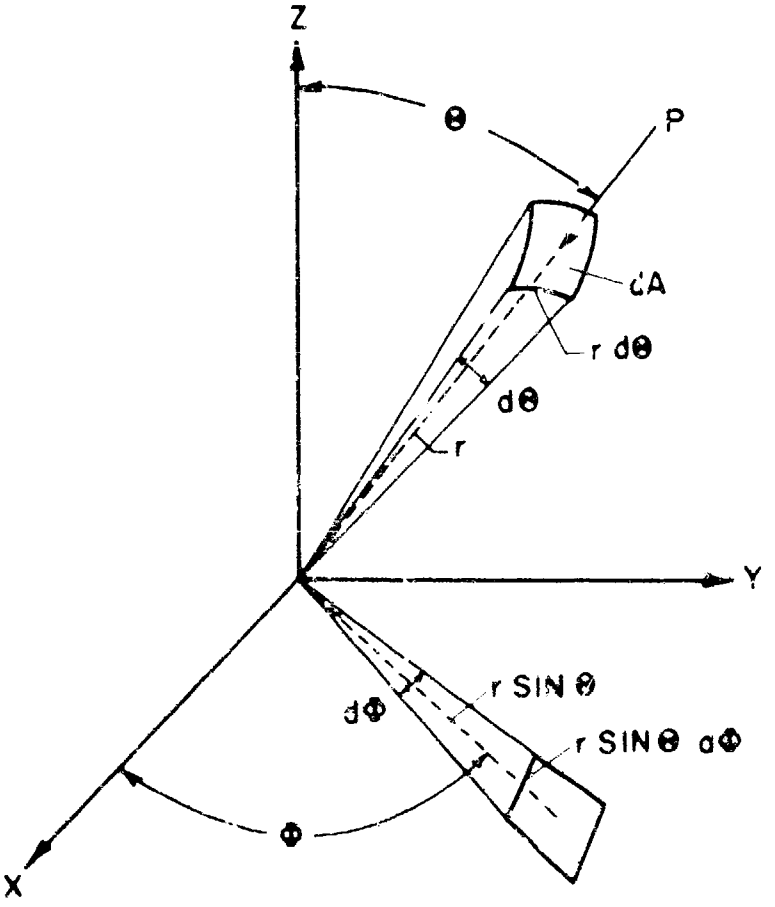

FIG. 2 DIFFERENTIAL SURFACE AREA OF A SPHERICAL DROPLET

The pressure variation across the droplet is assumed to be linear in the direction of flow (X-direction). Then,

$$P = (dp/dX)\ X$$

and

$$P_X = P \sin\vartheta \cos\phi$$

The pressure force acts in the negative direction in the quadrant shown. Then,

$$\begin{aligned} dF_X &= -P_X dA = -(P \sin\theta \cos\phi)\, dA \\ &= -(dp/dX)(X) \sin\theta \cos\phi\ (r^2 \sin\theta\, d\theta\, d\phi) \\ &= -(dp/dX)(r \sin\theta \cos\phi)\ r^2 \sin^2\theta \cos\phi\, d\theta\, d\phi) \\ &= -(dp/dX)\ r^3 \sin^3\theta\, d\theta \cos^2\phi\, d\phi \end{aligned} \tag{8}$$

Integrating equation 8,

$$\begin{aligned} F_X &= -(dp/dX)\ r^3 \int_0^{\pi} \int_0^{2\pi} (\sin^3\theta\, d\theta) \cos^2\phi\, d\phi \\ &= -(dp/dX)\ r^3 \int_0^{\pi} (\sin^3\theta\, d\theta)(\phi/2 + \sin 2\phi/4)\Big|_0^{2\pi} \\ &= (dp/dX)\ r^3 \pi \int_0^{\pi} \sin^3\theta\, d\theta \\ &= -(dp/dX)\ r^3 \pi \left[-\tfrac{1}{3}\cos\theta\ (\sin^2\theta + 2)\right]_0^{\pi} \\ &= -(dp/dX)\ r^3 \pi\ (4/3) \\ &= -(\text{volume of droplet})(dp/dX) \end{aligned}$$

therefore, the pressure force in the X-direction is,

$$F_P = -\forall_d \, (dp/dX) \tag{9}$$

where

dp/dX is negative, and

$\forall_d$ is the volume of a droplet.

Substituting equations 7 and 9 into equation 6 gives:

$$F_P + F_D = - (4/3) \pi r^3 (dp/dX) + (1/2) \bar{\rho}_G \pi r^2 \bar{V}_R^2 \bar{C}_D = m_d \bar{V}_L (dV_L/dX)$$

Substituting $(4/3 \pi r^3 \rho_L$ for m_d and dividing through by $(4/3) \pi r^3$ yields,

$$- (dp/dX) + (3/8) \bar{\rho}_G \bar{V}_R^2 \bar{C}_D / \bar{r} = \rho_L \bar{V}_L (dV_L/dX) \tag{10}$$

Rearranging equation 10,

$$dV_L = \frac{- dp}{\rho_L \bar{V}_L} \pm (3/8) \frac{\bar{\rho}_G \bar{V}_R^2 \bar{C}_D dX}{\rho_L \bar{V}_L \bar{r}} \tag{11}$$

The $\pm$ on the second term designates whether or not the drag on the droplet is positive or negative.

2-4.3 Continuity equation for the mixture

$$\dot{W}_T = \dot{W}_L + \dot{W}_G = \gamma_L A_L V_L + \gamma_G A_G V_G \tag{12}$$

or,

$$\dot{W}_L = \gamma_L A_L V_L \tag{13}$$

$$\dot{W}_G = \gamma_G A_G V_G \tag{14}$$

where

$\dot{W}_T$ = total mass rate of flow,

γ_L = specific weight of the liquid, and

γ_G = specific weight of the gas.

2-4.4 Equation of state for the gas

$$p = \gamma_G RT = \rho_G gRT \tag{15}$$

where

T = mixture temperature chosen, and

R = gas constant for air.

2-4.5 Defining equation for Reynolds number

$$N_R = \frac{\bar{\rho}_G \bar{V}_R \bar{d}_a}{\mu} = \frac{\text{inertial force}}{\text{viscous force}} \tag{16}$$

where

$\bar{d}_a$ = average droplet diameter, and

μ = viscosity of the gas.

2-4.6 Defining equation for Weber number

$$N_{We} = \frac{\bar{\rho}_G \bar{V}_R^2 \bar{r}}{\sigma} = \frac{\text{inertial force}}{\text{surface tension}} \tag{1}$$

Rearranging equation 13,

$$A_L = (\dot{W}_T/\gamma_L)(1/V_L)$$

and differentiating gives:

$$dA_L = - (\dot{W}_L/\gamma_L)(dV_L/V_L^2) = - \bar{A}_L (dV_L/\bar{V}_L) \quad (17)$$

$$A_T = A_L + A_G \quad (18)$$

Differentiating equation 18 and rearranging terms,

$$dA_G = dA_T - dA_L \quad (19)$$

Differentiating equation 15 with T held constant and rearranging terms,

$$d\rho_G = dp/gRT \quad (20)$$

Rearranging equation 14, differentiating, and substituting

$$\dot{W}_G = \bar{\gamma}_G \bar{A}_G \bar{V}_G$$

yields

$$dV_G = - \bar{V}_G (d\rho_G/\bar{\rho}_G) - \bar{V}_G (dA_G/\bar{A}_G) \quad (21)$$

Summarizing the above equations:

$$dp = \frac{\rho_L \bar{A}_L \bar{V}_L \, dV_L + \bar{\rho}_G \bar{A}_G \bar{V}_G \, dV_G}{- \bar{A}_T} \quad (9)$$

$$dV_L = \frac{\pm dF}{\rho_L \bar{A}_L \bar{V}_L} \pm (3/8) \frac{\bar{\rho}_G \bar{V}_R^2 C_D \, dx}{\rho_L \bar{V}_L \bar{r}} \quad (11)$$

$$N_R = \bar{\rho}_G \bar{V}_R \bar{d}_d / \mu \quad (16)$$

$$dA_L = - \bar{A}_L (dV_L/\bar{V}_L) \quad (17)$$

$$N_{We} = \bar{\rho}_G \bar{V}_R^2 \bar{r}/\sigma \tag{1}$$

$$dA_G = dA_T - dA_L \tag{19}$$

$$d\rho_G = dp/RTg \tag{20}$$

$$dV_G = - \bar{V}_G \left(d\rho_G/\bar{\rho}_G\right) - \bar{V}_G \left(dA_G/\bar{A}_G\right) \tag{21}$$

These are the equations in the forms utilized to determine the flow characteristics. All equations must be made dimensionally correct before calculations are performed. These equations were programmed for solution on an RPC 4000 digital computer.

2-5 Theoretical Nozzles Investigated

The gas viscosity and liquid surface tension were considered to be functions of temperature only and were therefore held constant.

Two nozzle configurations were investigated. Both configurations had the same inlet, throat, and exit areas, throat radius and converging angle. Table 2 lists the data employed in the analysis and the physical dimensions of the nozzles.

Figure 3 is a plot of total nozzle flow area as a function of axial length for nozzles I and II.

Table 2

Data Employed in Analysis
and Physical Dimensions of Nozzles

Average temperature of mixture	$504^{\circ}R$
Viscosity of air	3.68×10^{-7} slugs/ft-sec
Surface tension of water	0.0050 lb/ft
Inlet pressure	514.7 psia
Assumed initial droplet diameter	0.020 in.
Nozzle inlet area	3.287 in^2
Nozzle throat area	0.267 in^2
Nozzle exit area	2.45 in^2
Total converting angle	20°
Throat radius	1.0 in.
Diverging angle	
Nozzle I	7°
Nozzle II	21°
Mixture ratios employed	
Nozzle I	0.10 and 0.15
Nozzle II	0.10

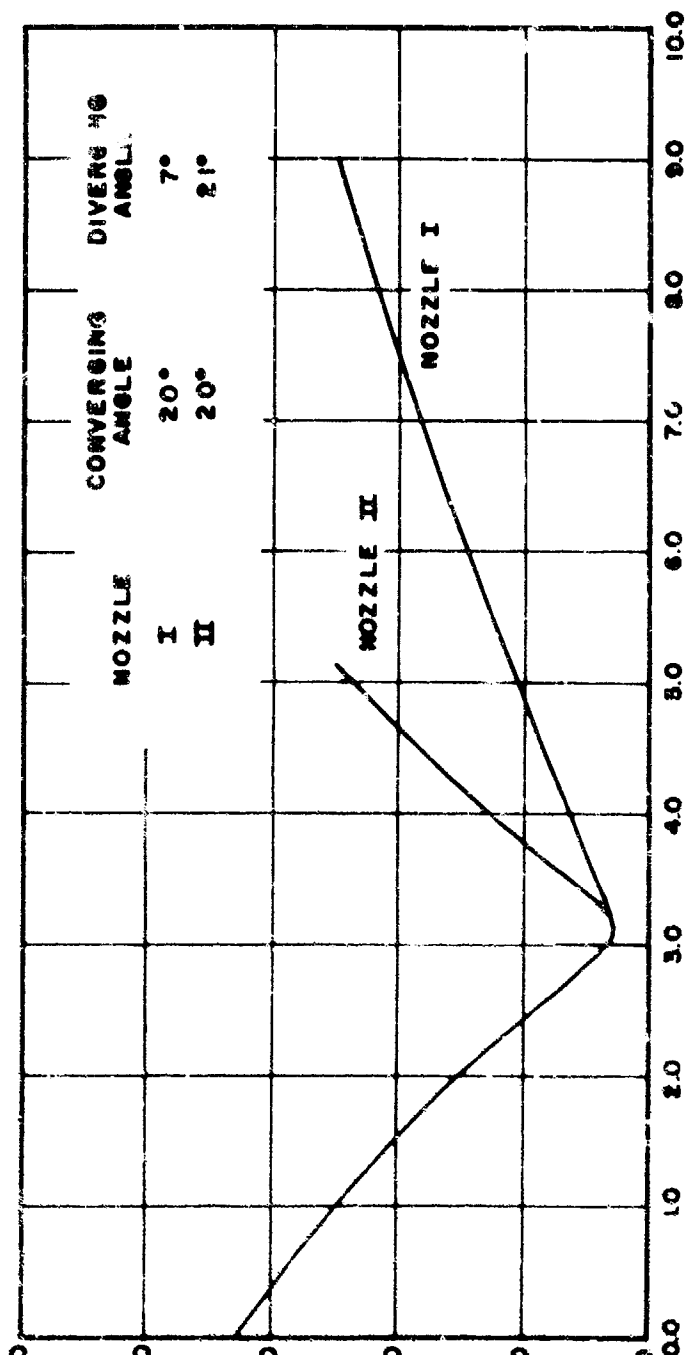

FIG. 3 AXIAL VARIATION OF NOZZLE AREA

2-6 Method of Solution

Numerical iteration was used with the above listed equations in order to determine the flow parameters as functions of the axial length of the nozzle. Small increments of length were taken along the nozzle axis, and through each increment the average value of each of the flow parameters was determined. The inlet conditions are the initial conditions for the first increment. After the flow parameters have been determined for the first increment, the values of the parameters at the exit of increment one are used as the initial values for the second increment and so on, until the exit section of the nozzle is reached.

When calculating the differentials of the flow parameters with the above listed equations, average values of the parameters are used in many of the expressions. When performing the calculations for the first time for a given increment, the average value of each of the parameters is not known and therefore the initial values of the parameters are used for the average values.

After the differential equations have been solved the first time for a given increment, an average value of each parameter can be calculated as follows:

$$\bar{Z} = Z_i + dZ/2$$

where

$\bar{Z}$ = the average value of a flow parameter,

Z_i = initial value of the flow parameter at the beginning of any increment, and

dZ = differential value of the parameter calculated with the corresponding equation.

The equations are again solved for the same increment, but this time using the average values which have been calculated. This process is repeated as many times as is necessary (for each increment) to obtain the desired accuracy of each of the flow parameters at the exit of the increment. The value of a parameter at the exit of a given increment is found by adding the differential quantity to the initial value.

Small increments were taken along the fixed geometric shapes chosen and therefore, the total flow area for each increment is known.

The accuracy to which the parameters are calculated effects the end results since all errors are multiplied when proceeding from increment to increment. All calculations in this analysis were made with an accuracy of 0.10%.

The size of the increment employed greatly effects the results obtained. It was necessary to determine the smallest increment that should be taken in order that the calculated parameters would not change at a given section of the nozzle if a still smaller increment were employed. This increment size was determined to be approximately twice the diameter of the droplet in length at any position.

Seven significant figures of accuracy of the inlet conditions were not sufficient to allow the expansion to proceed to completion at 14.7 psia. For example, let the correct seventh significant figure of one of the parameters at the inlet be five. If a trial solution is attempted using four, the solution would begin to diverge in one direction (a pressure rise) at some point along the nozzle axis. If instead a six is tried, the solution would diverge in the other direction (a rapid pressure drop). The solution must be restarted at the inlet to the nozzle, with the new chosen

values of the inlet conditions (V_L, V_G, $\dot{M}_L$, $\dot{M}_G$), each time that the solution is found to diverge in either direction. The RPC 4000 digital computer, when employed with the Purdue Interpreter routine, could only be utilized to perform accurate calculations to seven significant figures.

After obtaining the correct seventh significant figure of each of the inlet conditions, the calculations were restarted at the point where divergence began in either direction. Integrated forms of the above derived equations were then utilized in an iterative form as discussed by D. L. Crabtree (2).

The Weber number (equation 1) was utilized to determine the average droplet size in any particular increment. The droplet was assumed to be of constant diameter through any increment at the average value determined. The Weber number was calculated at the nozzle inlet. If this calculated value was less than the critical Weber number of 6.3, the droplet remained constant in size for the first increment. For each increment the Weber number was determined and if it remained less than 6.3 the droplet did not undergo critical decomposition. The critical value is the maximum value of the Weber number that can be attained. If the Weber number becomes equal to or greater than 6.3, a new droplet radius is calculated using a value of 6.3 for the Weber number in equation 1.

Figure 4 is a block diagram of the computer program utilized in this analysis. The following parameters were printed out for each increment; X, V_L, V_G, r, N_{We}, N_R. Figures 5, 6, and 7 are plots of the predicated variations in the flow parameters with axial nozzle length for nozzles I and II.

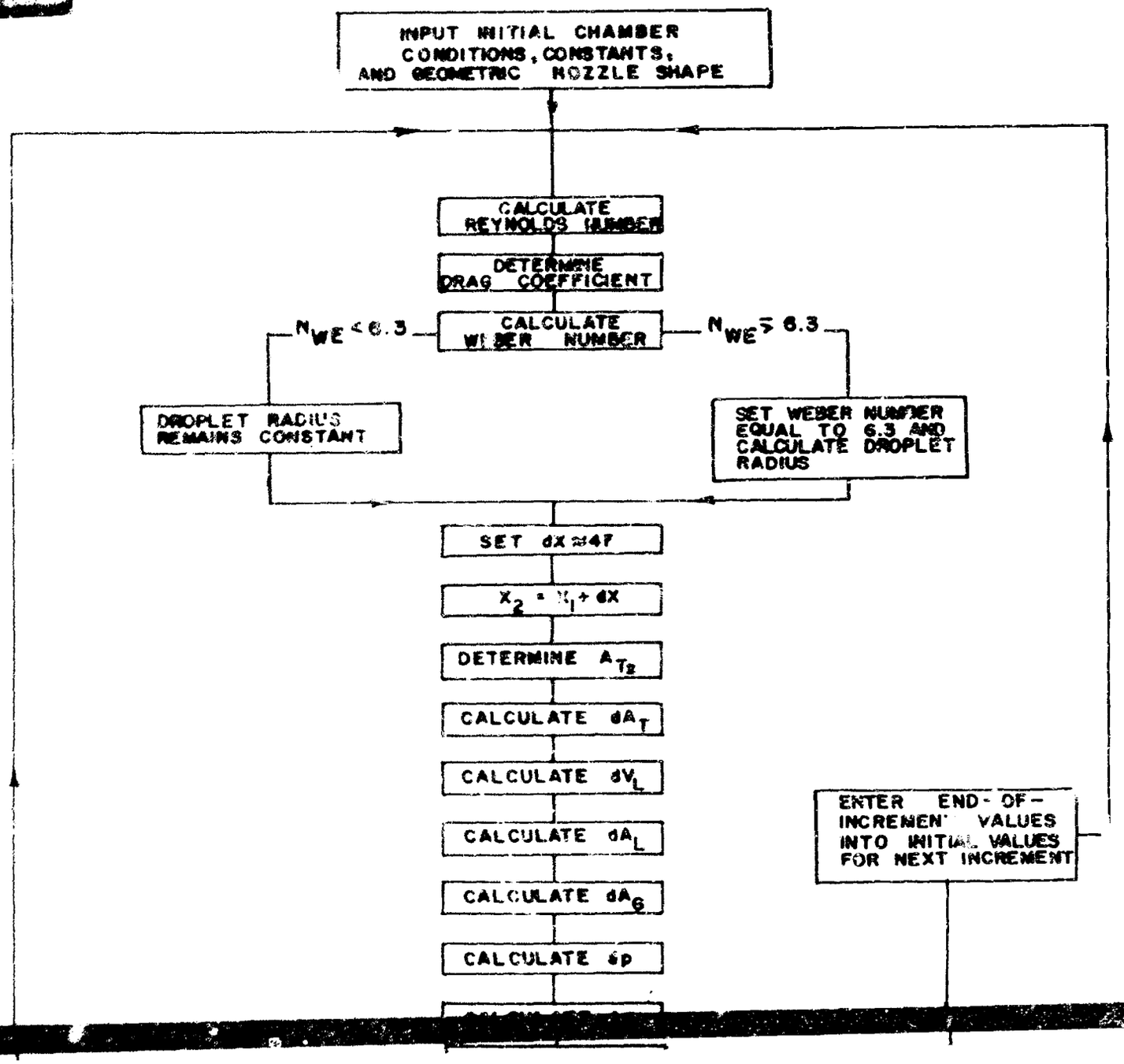
INPUT INITIAL CHAMBER CONDITIONS, CONSTANTS, AND GEOMETRIC NOZZLE SHAPE
CALCULATE REYNOLDS NUMBER
DETERMINE DRAG COEFFICIENT
CALCULATE WEBER NUMBER
$N_{WE} < 6.3$
$N_{WE} \geq 6.3$
DROPLET RADIUS REMAINS CONSTANT
SET WEBER NUMBER EQUAL TO 6.3 AND CALCULATE DROPLET RADIUS
SET $dX \approx \Delta r$
$X_2 = X_1 + dX$
DETERMINE A_{T_2}
CALCULATE dA_T
CALCULATE dV_L
CALCULATE dA_L
CALCULATE dA_G
CALCULATE δp
ENTER END-OF-INCREMENT VALUES INTO INITIAL VALUES FOR NEXT INCREMENT

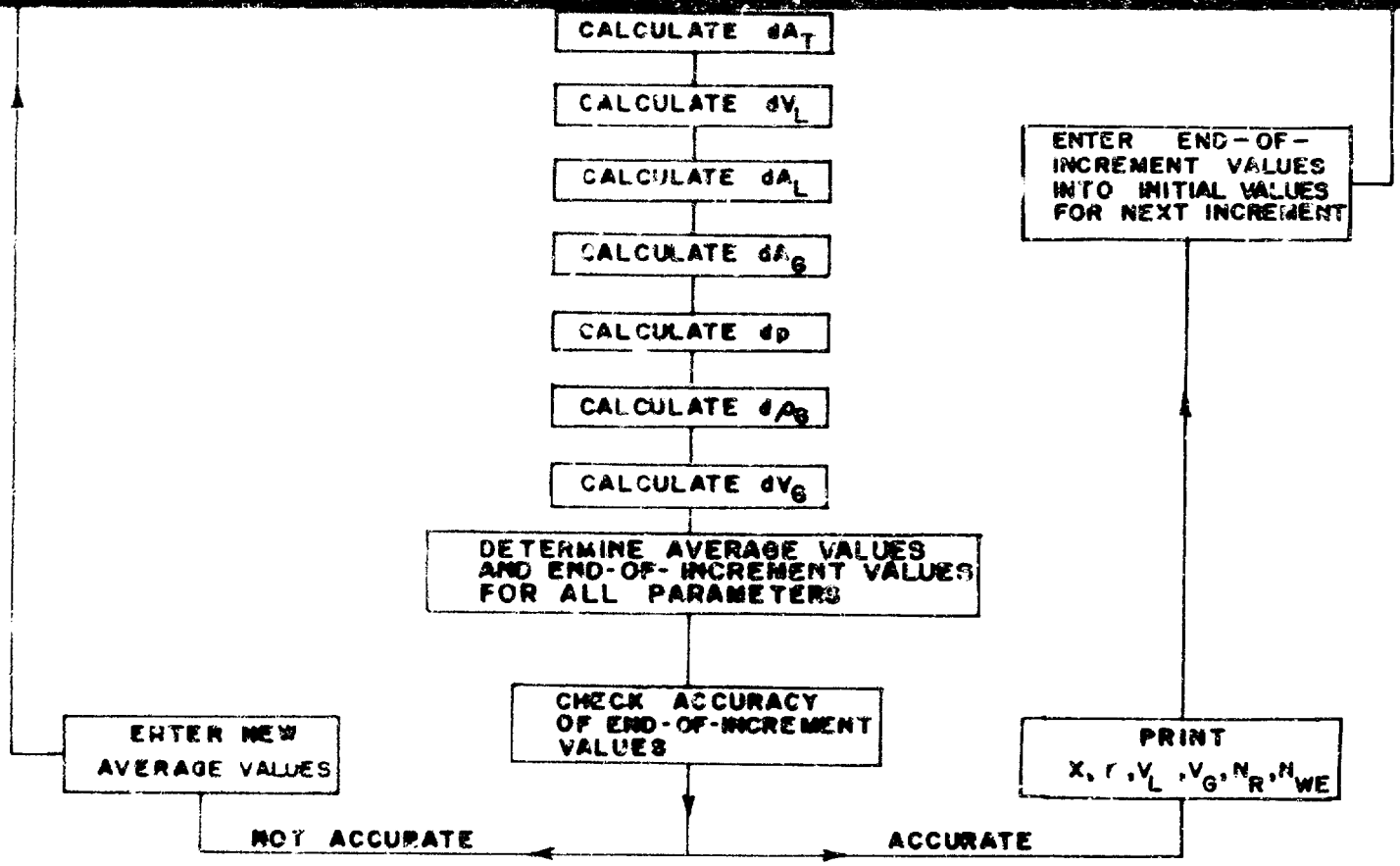

FIG. 4 BLOCK DIAGRAM OF COMPUTER PROGRAM

FIG. 5 CALCULATED FLOW PARAMETERS
AS A FUNCTION OF THE AXIAL DIS

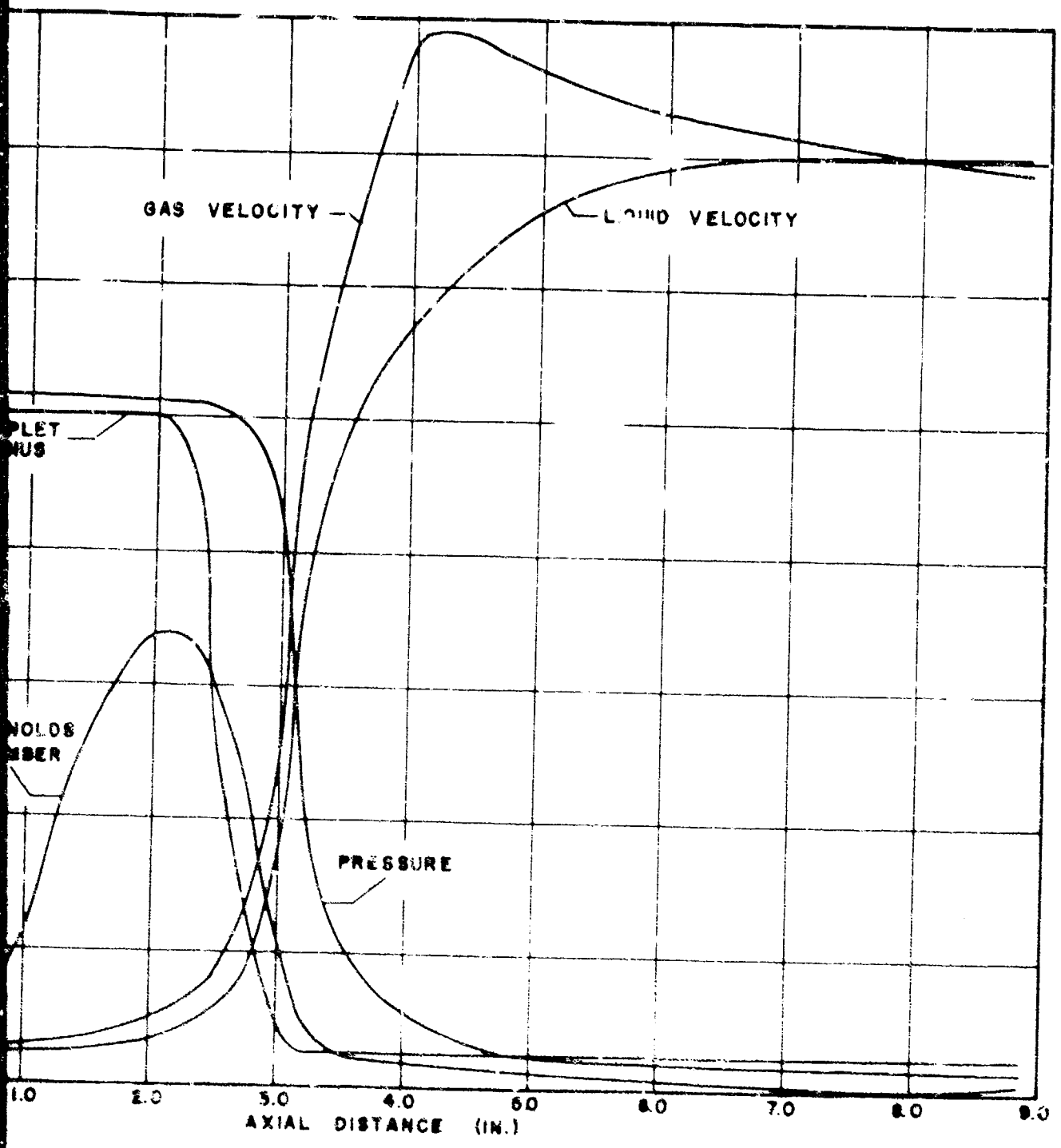

ATED FLOW PARAMETERS FOR NOZZLE I ($W_g/W_L = 0.10$)
UNCTION OF THE AXIAL DISTANCE ALONG THE NOZZLE

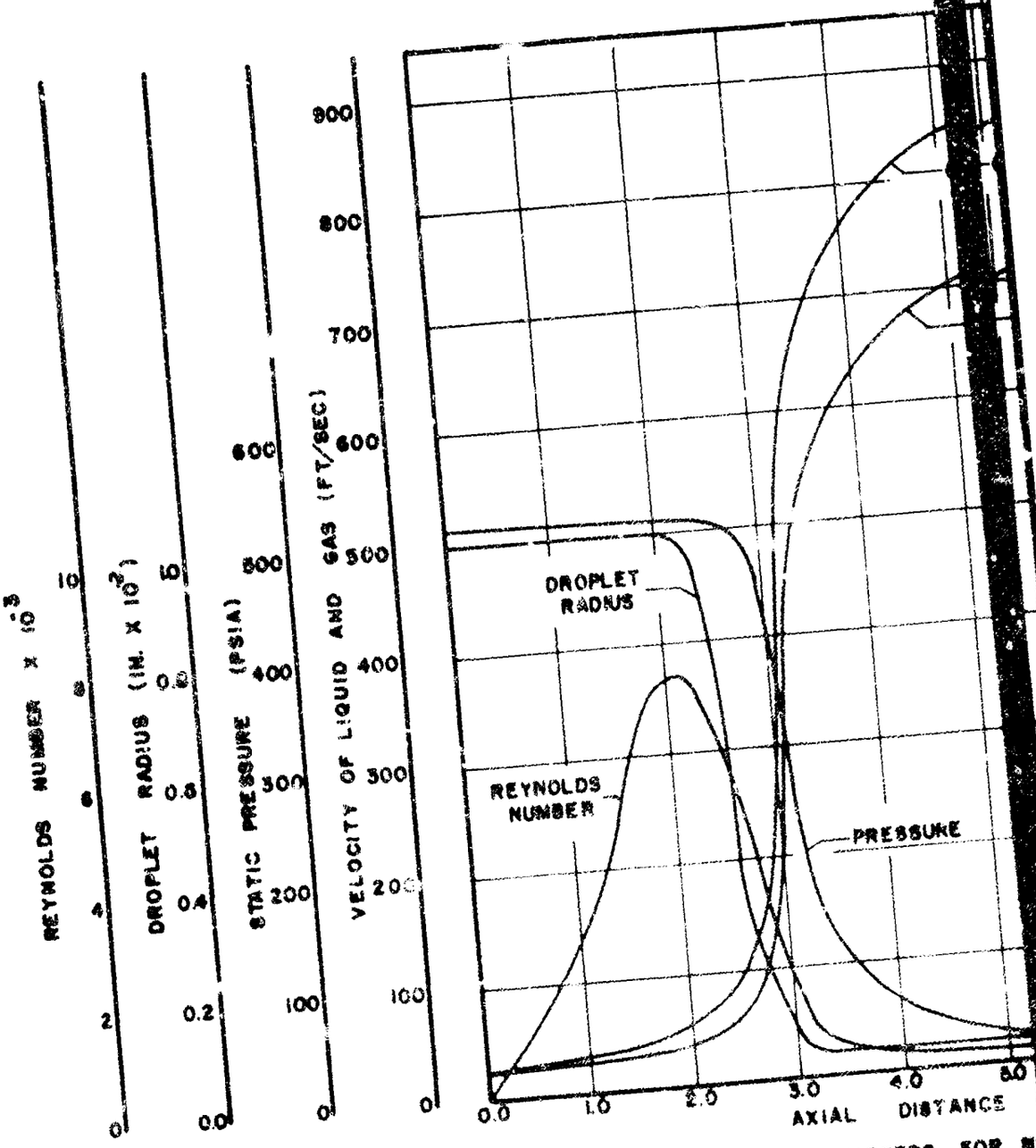

FIG. 6 CALCULATED FLOW PARAMETERS FOR N
AS A FUNCTION OF THE AXIAL DISTANCE

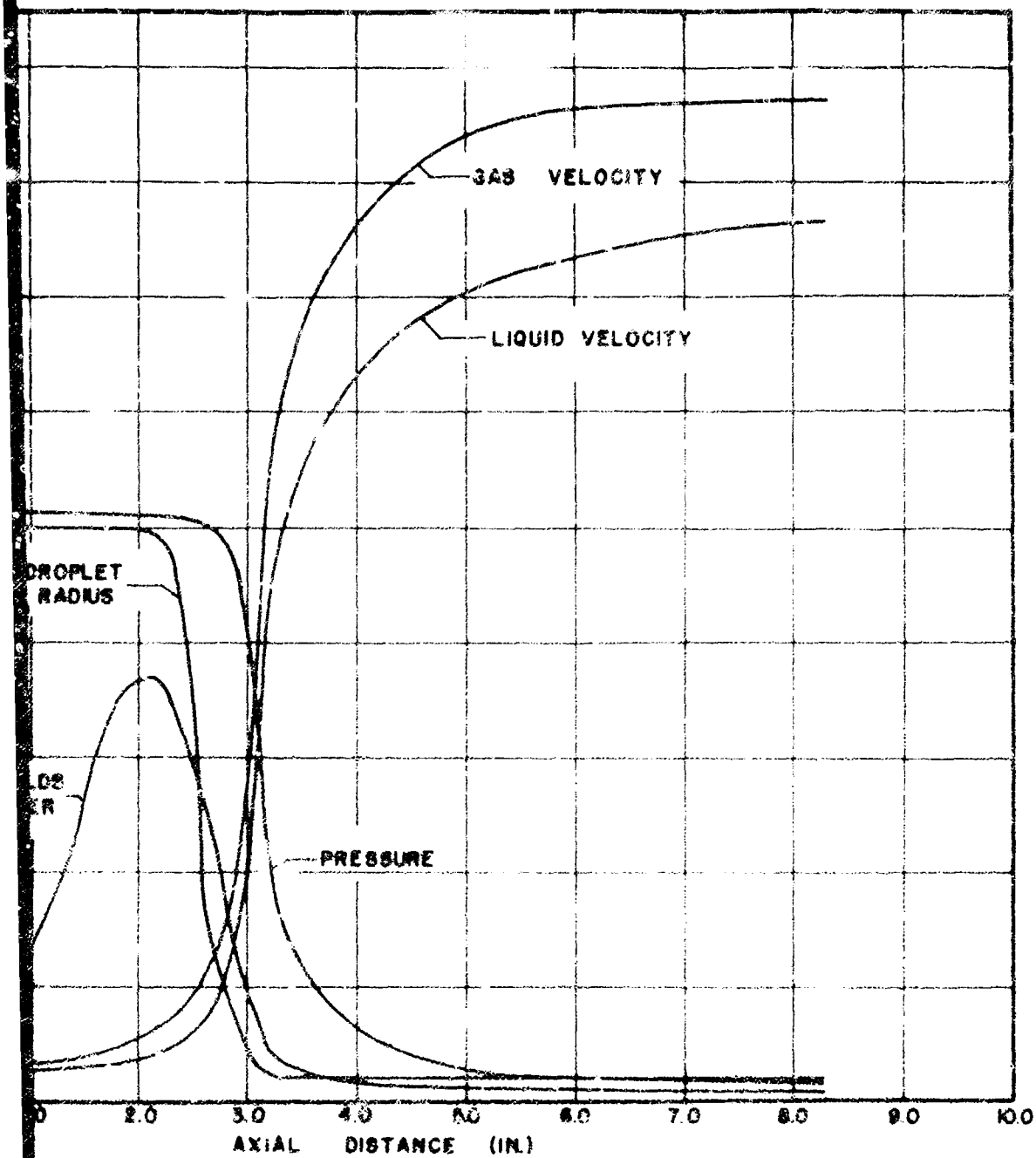

CALCULATED FLOW PARAMETERS FOR NOZZLE I ($W_g/W_l = 0.18$)
AS A FUNCTION OF THE AXIAL DISTANCE ALONG THE NOZZLE

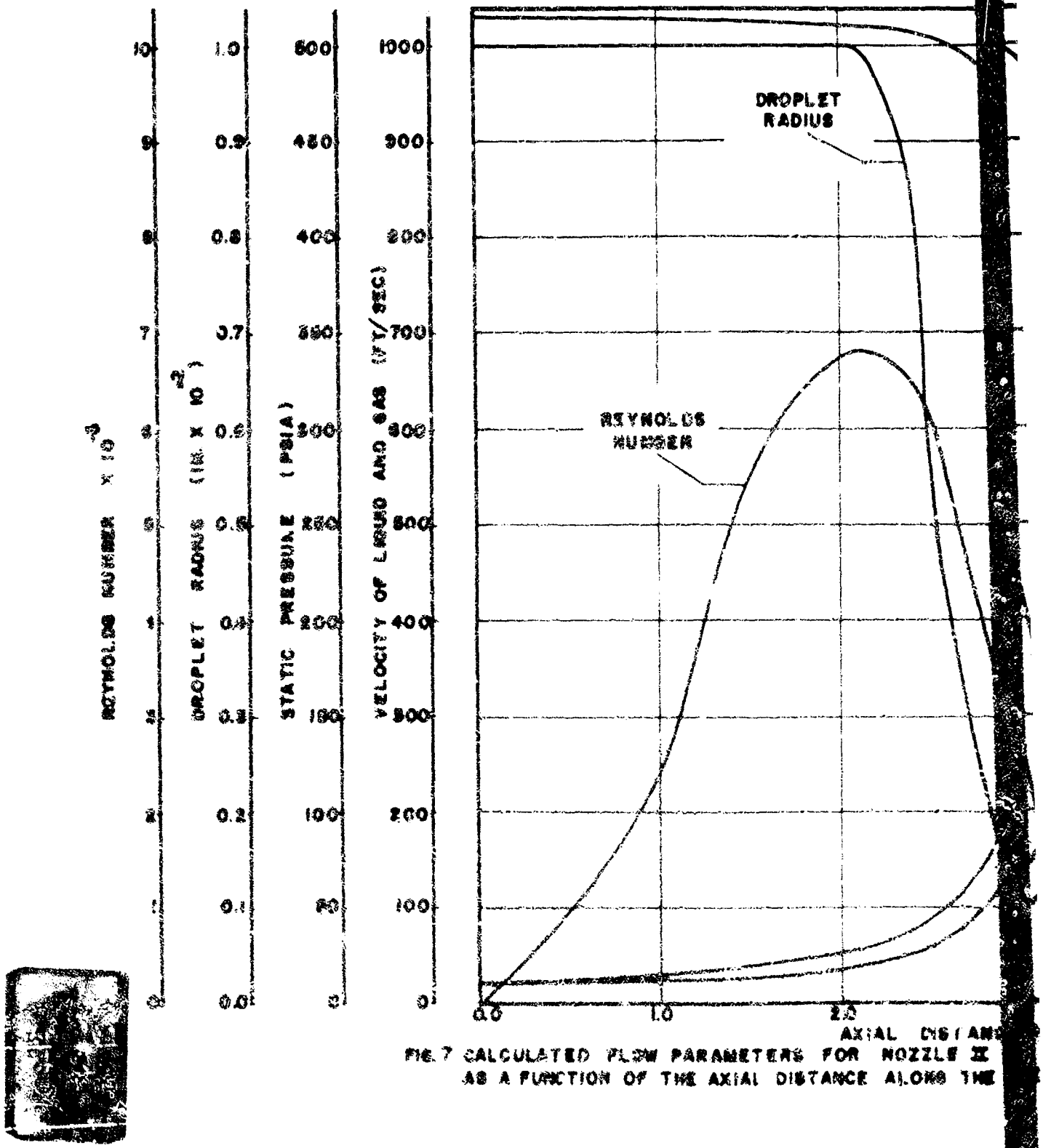

FIG. 7 CALCULATED FLOW PARAMETERS FOR NOZZLE II AS A FUNCTION OF THE AXIAL DISTANCE ALONG THE

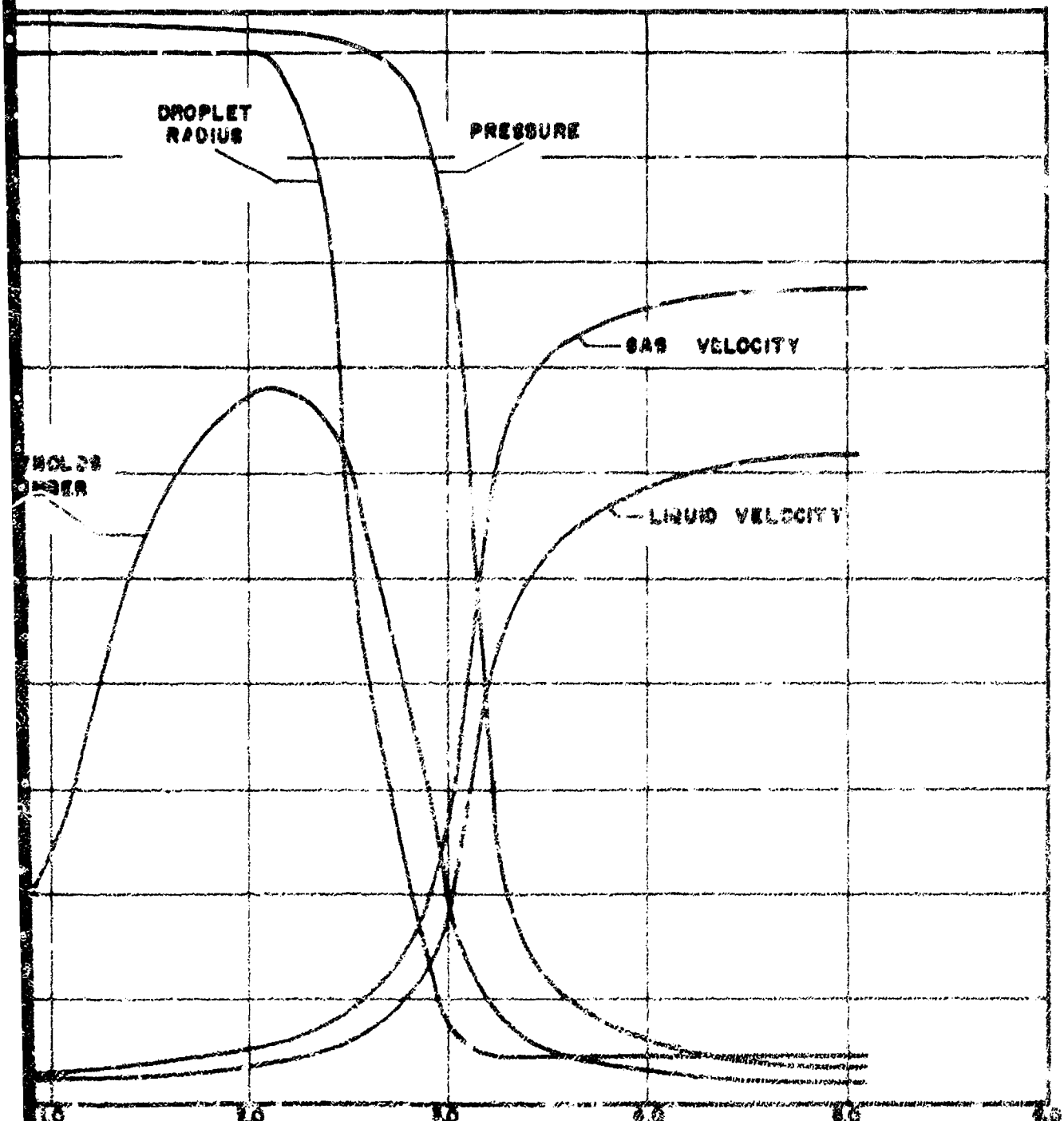

PARAMETERS FOR NOZZLE IX ($W_i/W_o = 0.10$)
THE AXIAL DISTANCE ALONG THE NOZZLE

3 EXPERIMENTAL VERIFICATION

3-1 Description of Experimental Nozzles

In order to verify the theoretical predictions, experimental nozzles were constructed. The experimental nozzles were annular in shape and were constructed with the same area vs. axis length as the nozzles investigated theoretically.

Figure 8 is a photograph of the component parts of the experimental nozzle and Figure 9 presents a cross-sectional view of one of the assembled experimental nozzles. The injector was the same type as used by D. I. Crabtree (2). The water was injected through small tubes with an annular flow of air around each tube. To insure that the streams emitting from the injector are broken into droplets, a stainless steel screen was placed in the path of flow approximately three inches from the injector face. Another two inches were allowed before the converging portion of the nozzle began in order to stabilize the flow.

3-2 Description of Test Facility

Figure 10 is a photograph of one of the experimental nozzles mounted on the thrust stand. The 1/8 in. tubes which are soldered to the outer nozzle casing were utilized to determine the pressure profile along the nozzle axis. Each 1/8 in. tube leads to a 0.060 in. pressure tap drilled through the outer nozzle casing. Each of the tubes soldered to the nozzle casing was connected to a common manifold through needle valves.

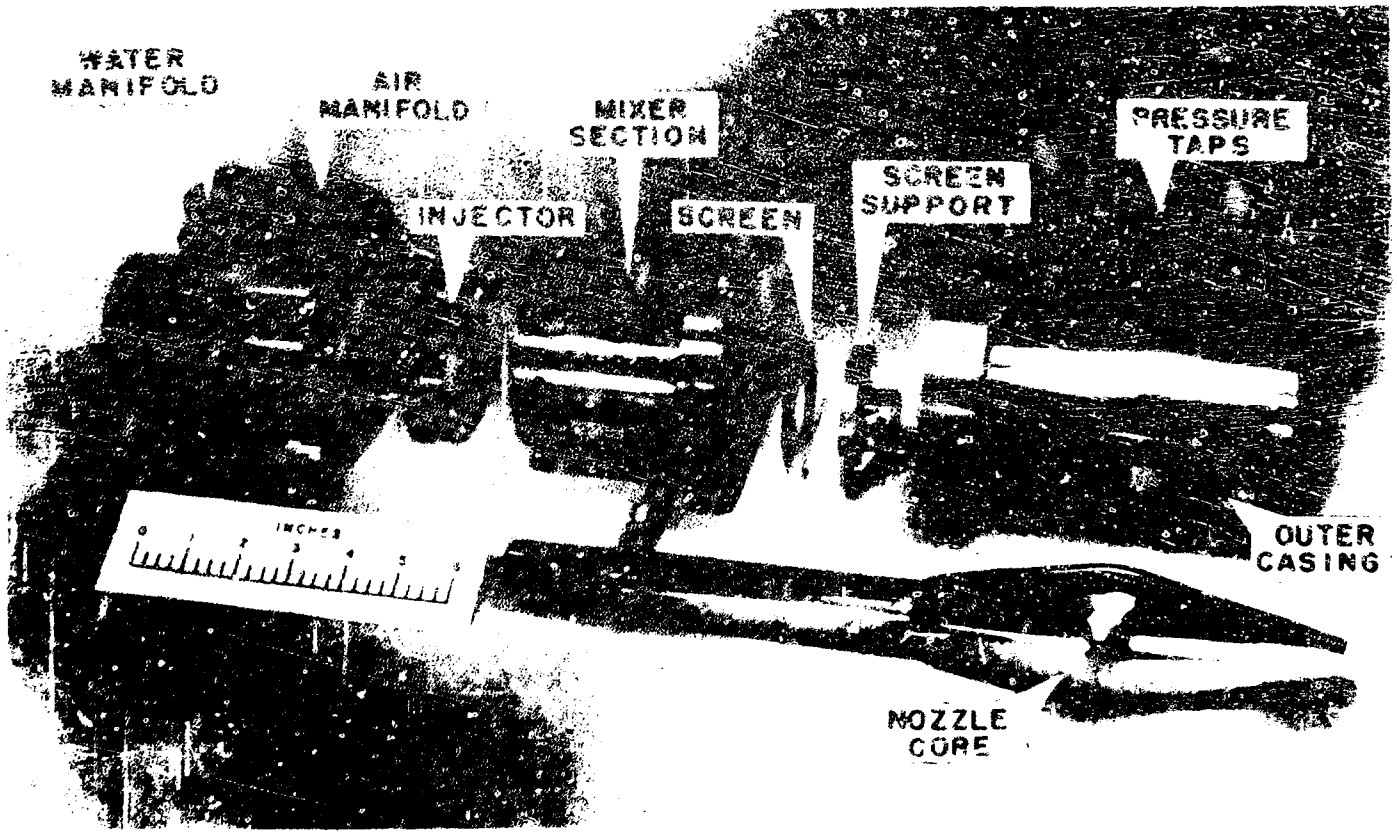

FIG. 8 EXPERIMENTAL NOZZLE COMPONENTS

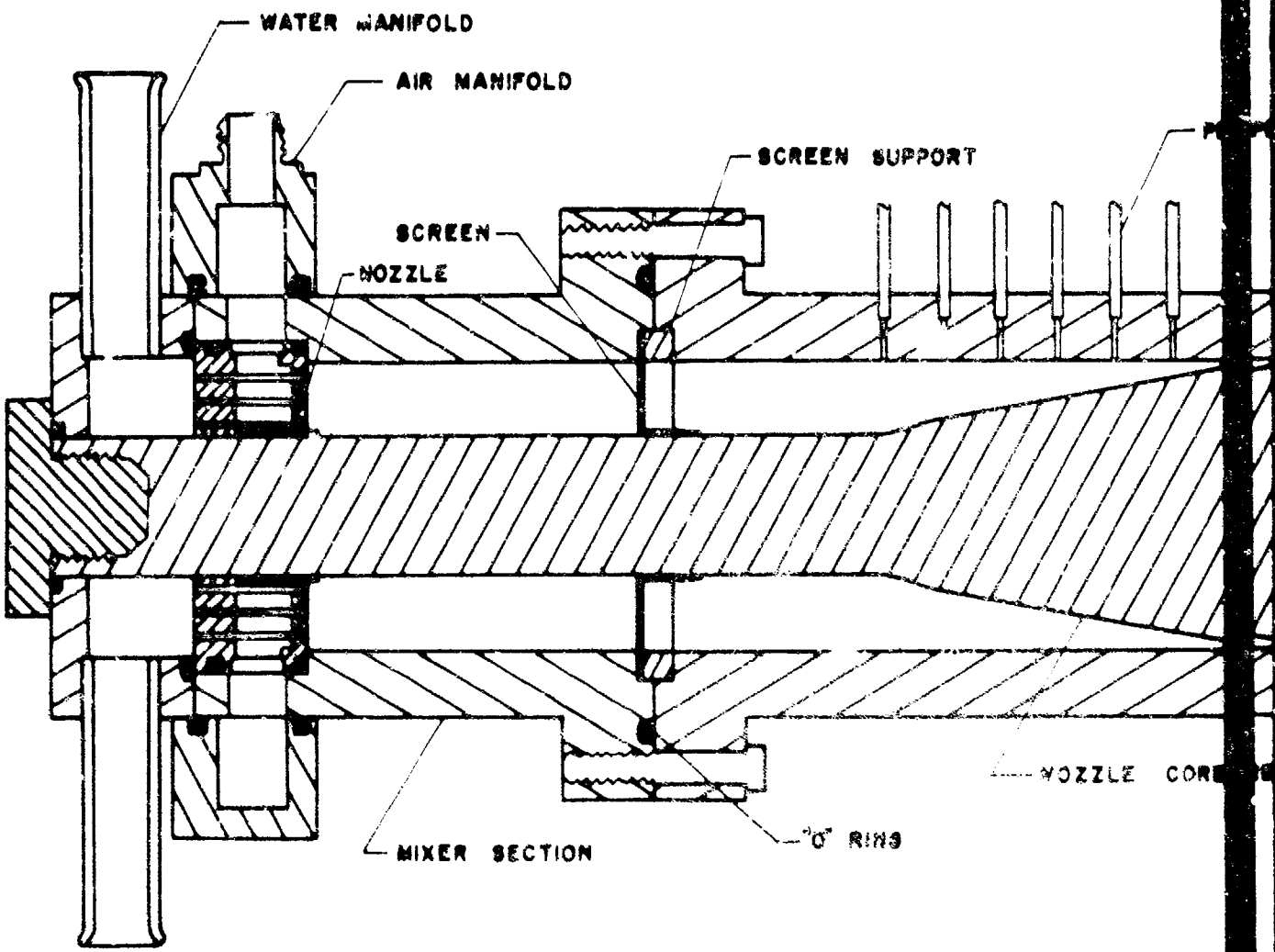

FIG. 9 CROSS-SECTIONAL VIEW OF THE EXPERIMENTAL NOZZLE

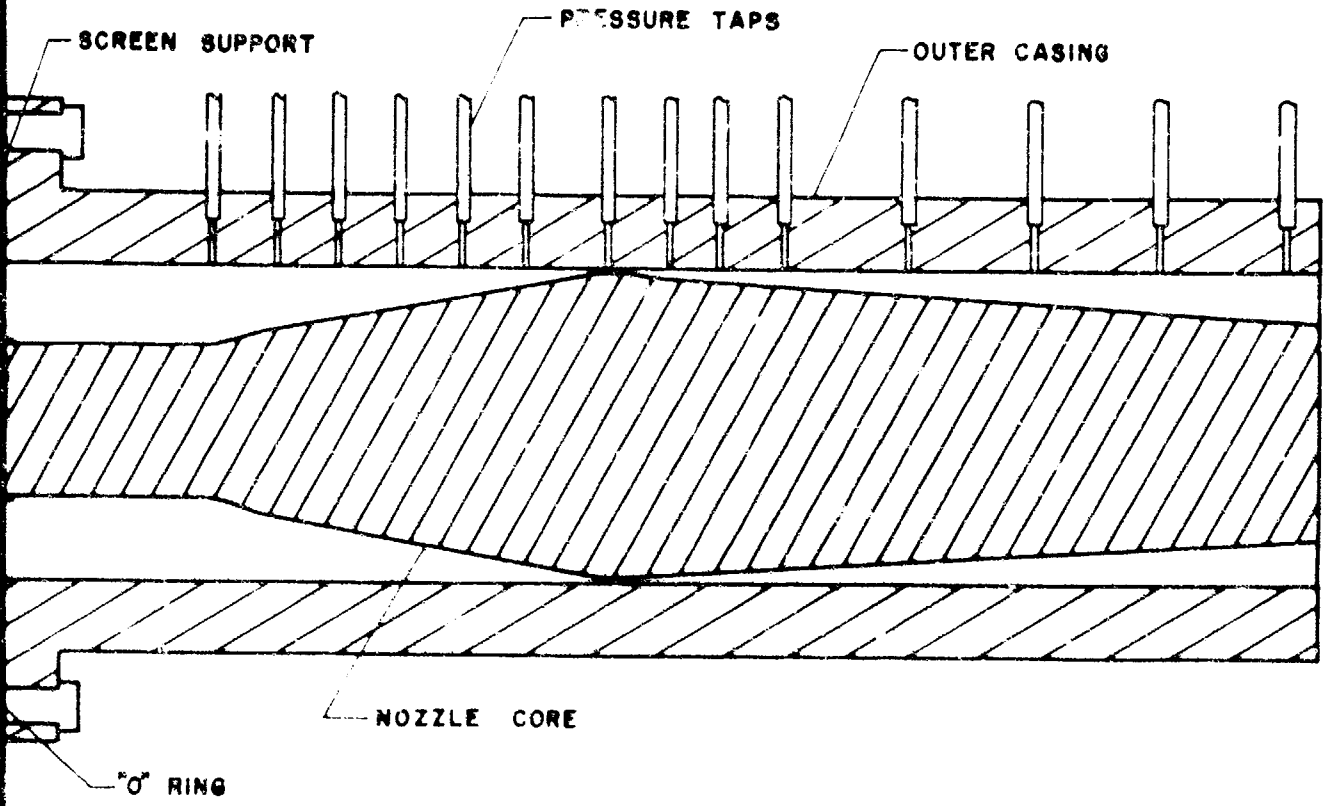

VIEW OF THE EXPERIMENTAL NOZZLE

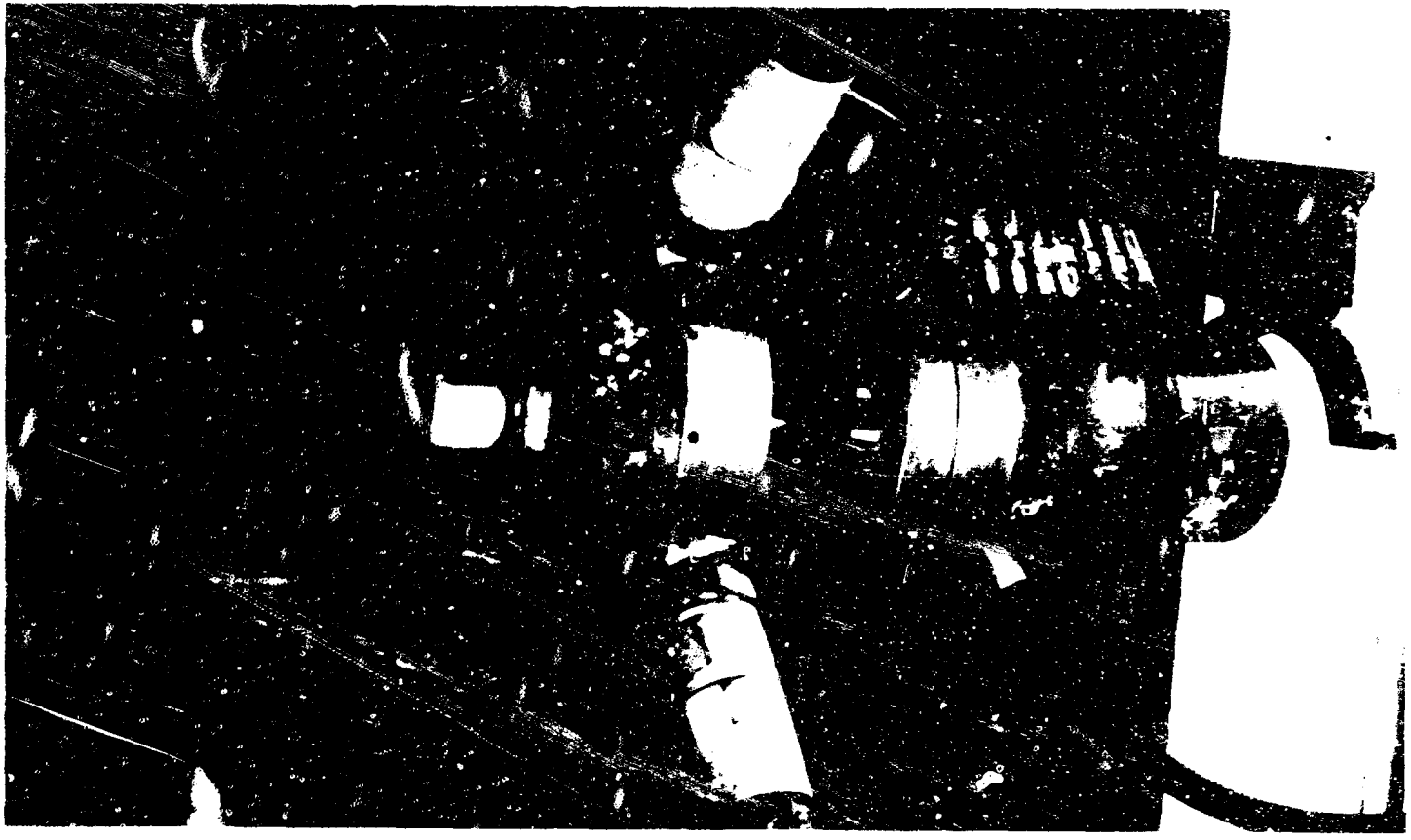

FIG.10 EXPERIMENTAL NOZZLE MOUNTED ON THRUST STAND

The pressure at a particular tap was measured by opening the corresponding needle valve and recording the manifold pressure. The manifold pressure was measured by a Wiancko pressure transducer and was recorded on a Brown strip-chart recorder.

Figure 11 is a schematic diagram of the facility utilized in the experimental investigation.

The nozzle was mounted on a vertical beam, pivoted at the upper end as shown in Figure 11. The thrust of the nozzle was measured with a Wiancko force transducer and recorded on a Brown strip-chart recorder.

Water was supplied to the nozzle at pressures between 500 and 1000 psig. from four tanks which have a 5200 lb. capacity. The water flow rate was measured by a 5/8 in. sharp-edged orifice. The pressure drop across the orifice was measured with a Wiancko pressure transducer and recorded on a Brown strip-chart recorder. A milliameter was located on the control panel which received a signal from the Brown recorder to indicate the liquid flow rate. The liquid flow rate was controlled with an Annin Domotor valve and the temperature of the water in the supply line was measured with an iron-constantan thermocouple.

Air was supplied to the nozzle from several banks of large storage tanks at pressures between 900 and 1300 psig. Grove type dome-loaded regulator valves were utilized to supply the nozzle with the desired pressure. The gas flow rate was measured by a 0.354 in. sharp-edged orifice. The pressure drop across the orifice and the pressure upstream of the orifice were measured with Wiancko pressure transducers and recorded on Brown strip-chart recorders. The temperature of the air

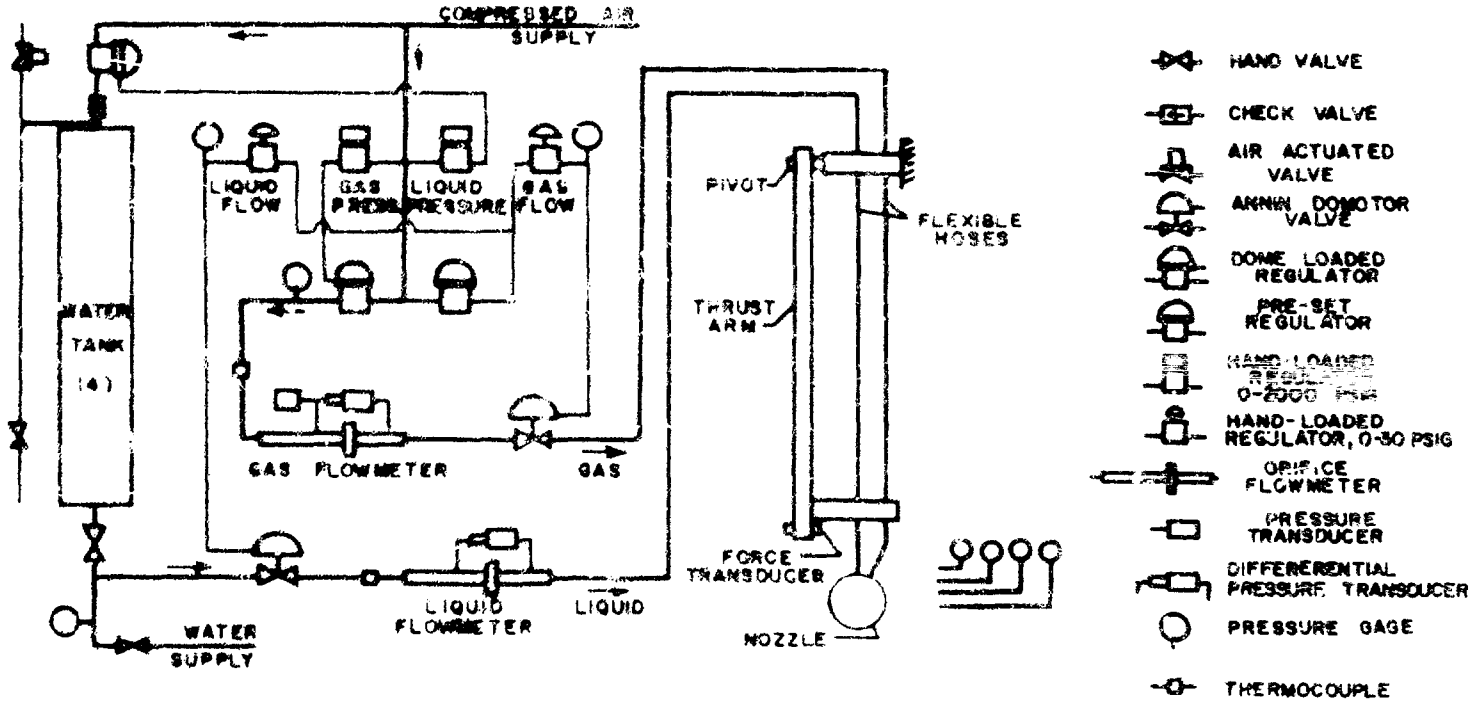

FIG. II SCHEMATIC DIAGRAM OF TEST FACILITY

upstream of the orifice was measured with an iron-constantan thermocouple and also recorded on a Brown strip-chart recorder. The air flow rate was controlled with an Annin Domotor valve and was indicated on the flow panel with a milliameter as was the liquid flow rate.

Both liquid and gas orifices were made and calibrated according to A.S.M.E. standards.

The pressure at the entrance of the converging portion of the nozzle was indicated on a Bourdon-tube pressure gage and was maintained at 500 psig.

The pressure and thrust transducers were calibrated immediately before and after each experimental run.

3-3 Experimental Data Accumulation

In the experimental investigation, mixture ratios of 0.08, 0.10, 0.12, and 0.15 were utilized with each nozzle. Four nozzles were utilized, each having a converging angle of 20°. Diverging angles of 7°, 14°, 21°, and 28° were employed. Numerous runs were made in order to insure that the results of the particular runs desired (those identical to the theoretical nozzle calculations) were valid. Data taken included the following:

1. liquid flow rate,
2. gas flow rate,
3. thrust,
4. liquid temperature,
5. gas temperature, and
6. pressure profile along nozzle axis.

The experimental nozzles which were identical to those investigated theoretically are listed in Table 3.

Table 3

Nozzles Employed in Both
Experimental and Theoretical Analyses

Nozzle	Converging Angle	Diverging Angle	Throat Area	Inlet Area	Exit Area
I	20°	7°	0.267	3.287	2.450
II	20°	21°	0.267	3.287	2.450

4 COMPARISON OF THEORETICAL AND EXPERIMENTAL RESULTS

4-1 Pressure Profiles

Figure 3 presents the flow areas of the two nozzles which were investigated both experimentally and theoretically.

In Figures 12, 13, and 14 the predicted pressure profiles are compared with those obtained experimentally. From Figures 12, 13, and 14 it can be seen that from the nozzle inlet into the diverging section, the measured pressure profiles were practically identical with the predicted profiles in all three cases investigated. In each of the three cases the experimental pressure profile dropped below the theoretical profile in the diverging portion of the nozzle.

In the diverging portion of the nozzle both phases are rapidly approaching their maximum velocities. In this region of high liquid and gas velocities, the quantity of heat transferred in a small finite period of time is minute and the pressure drops faster for the real case than for the isothermal model. As the pressure drop per unit length becomes small in the latter portion of the diverging section the pressure curves again match quite closely. By the time that the mixture has traversed the entire diverging section, the liquid has had sufficient time to transfer some heat to the gas.

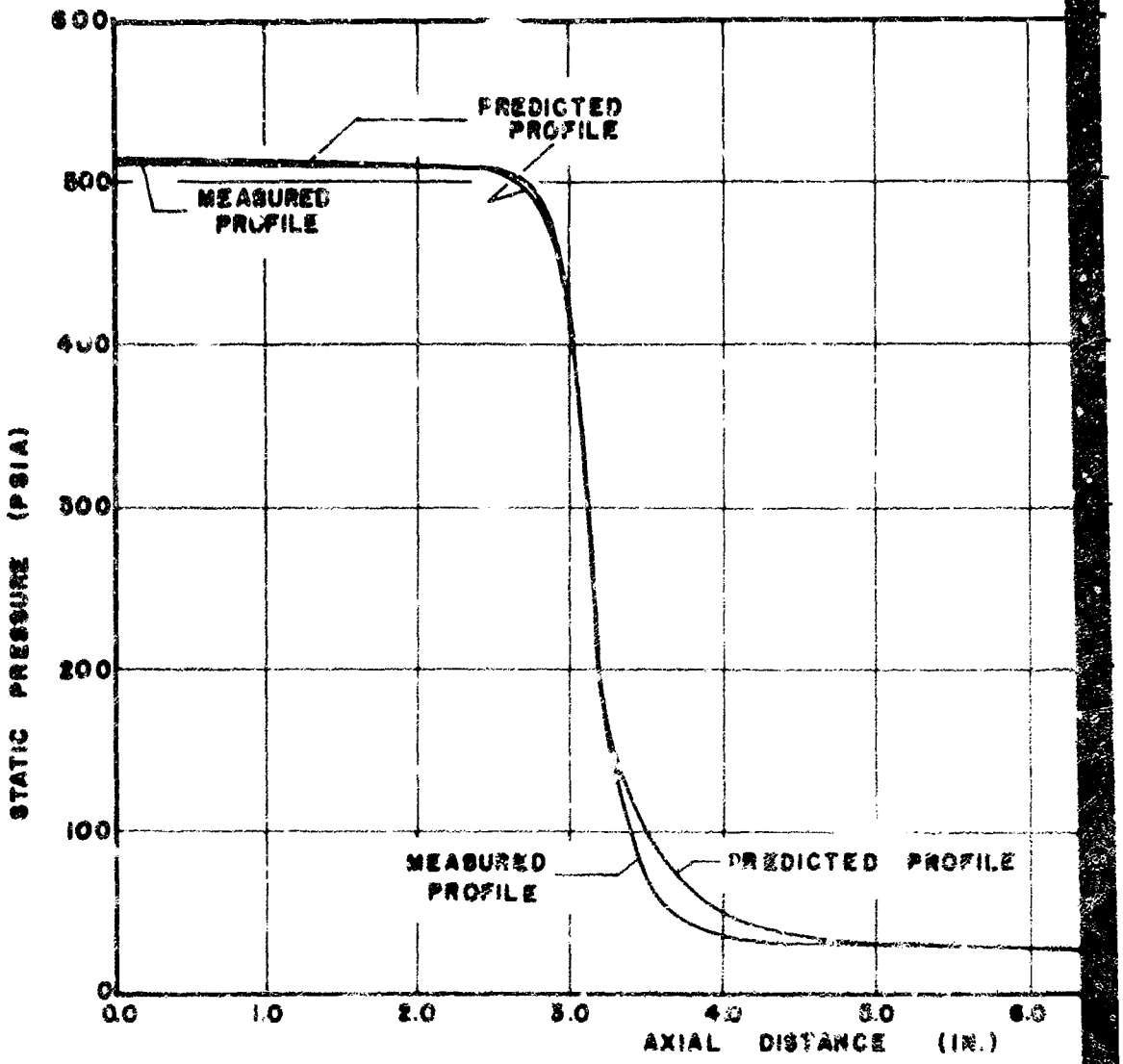

FIG. 12 PREDICTED AND MEASURED STATIC PRESSURE PROFILES FOR NOZZLE I (W_s/W_L = 0.10)

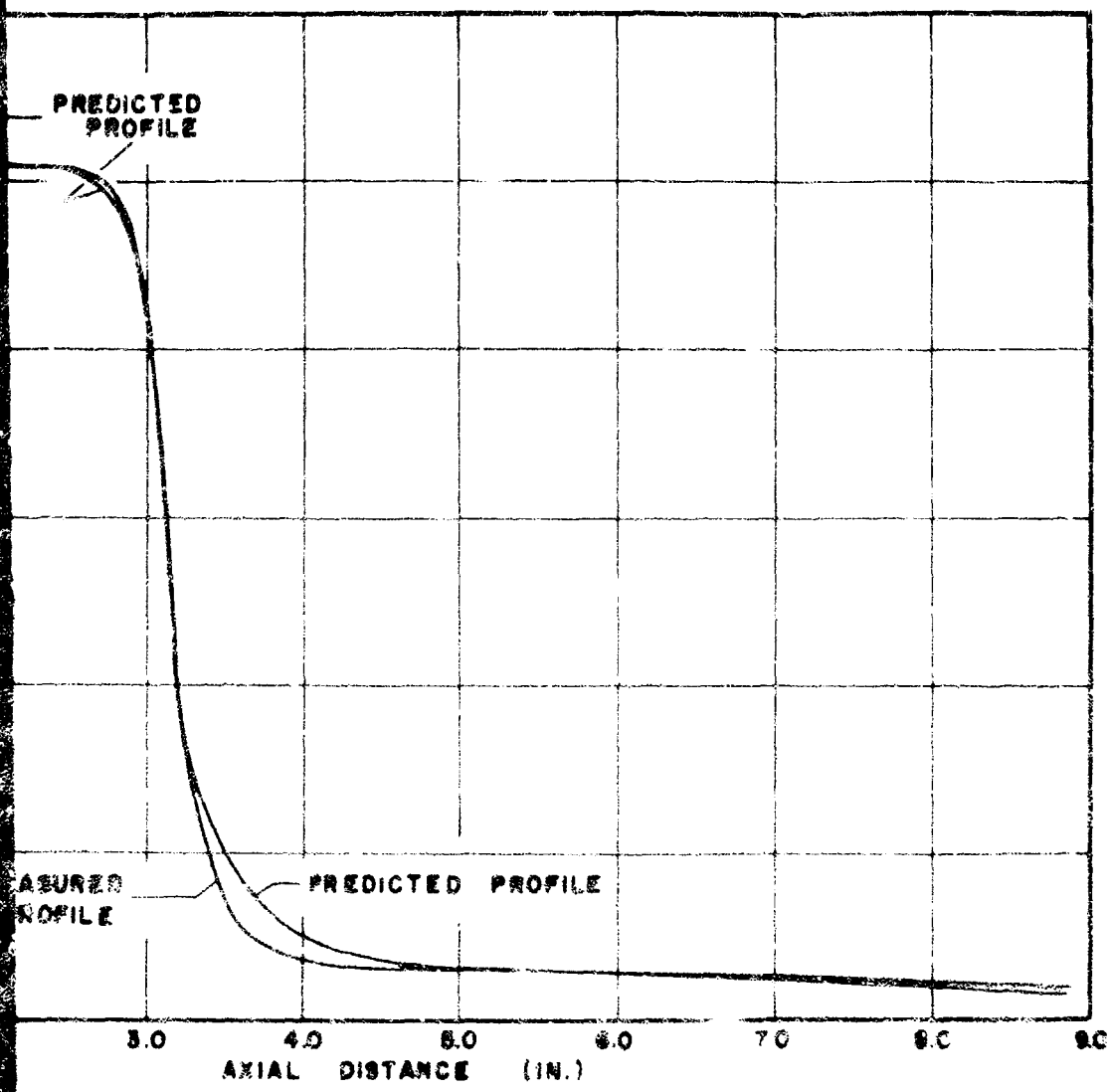

CTED AND MEASURED STATIC PRESSURE
ROFILES FOR NOZZLE I (r_w/W_L = 0.10)

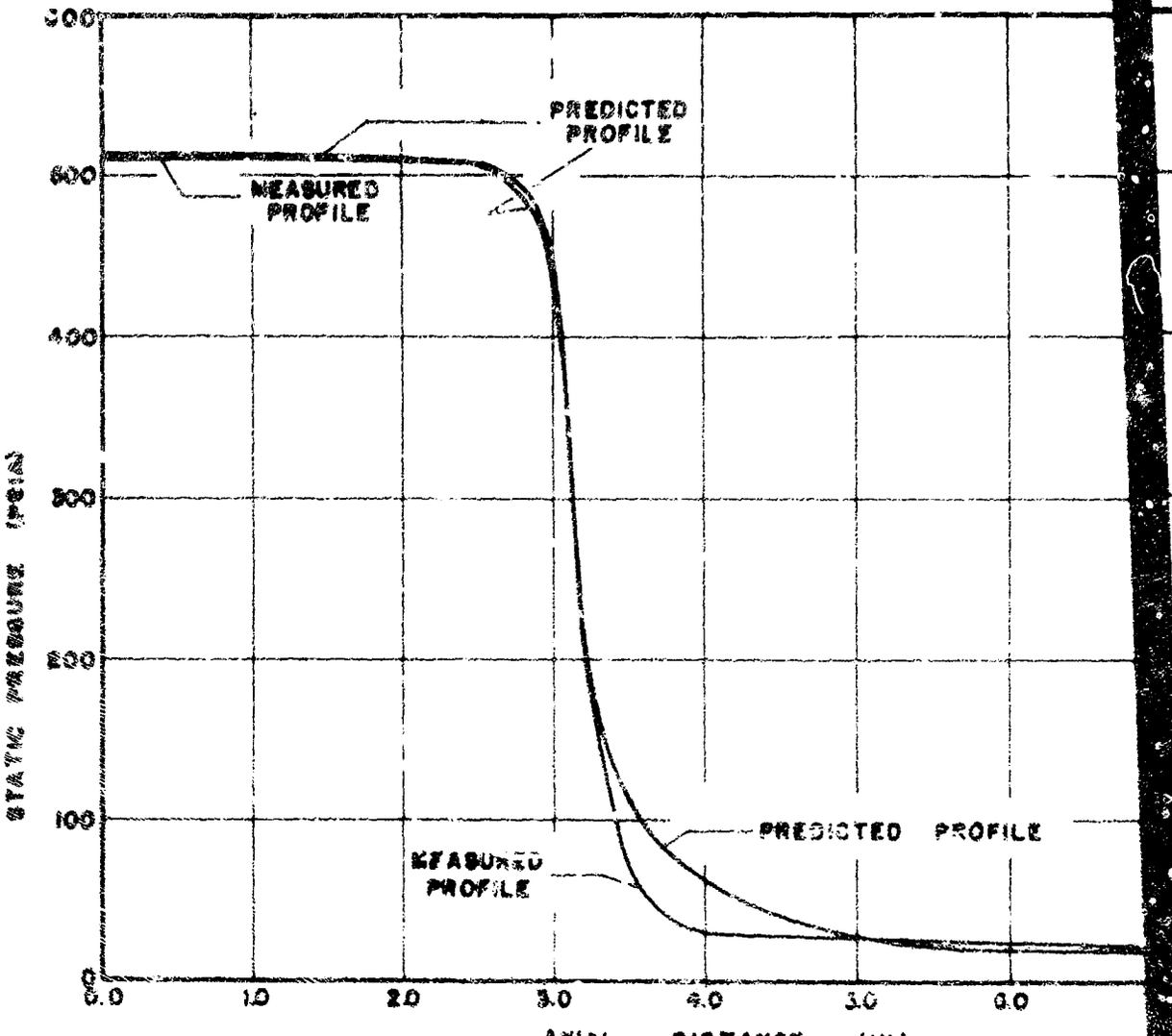

FIG. 13 PREDICTED AND MEASURED STATIC PRESSURE PROFILES FOR NOZZLE I ($W_s/W_p = 0.18$)

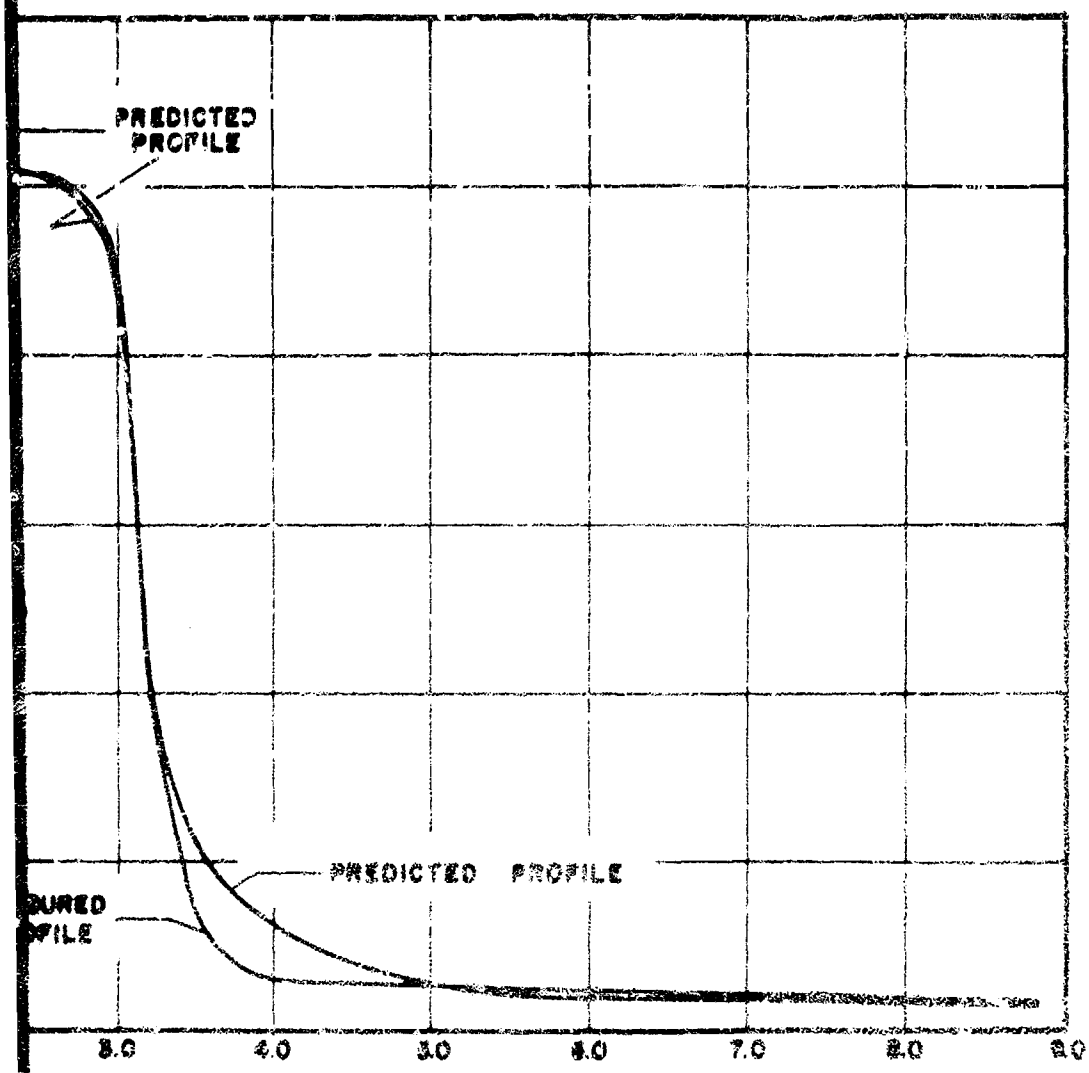

TED AND MEASURED STATIC PRESSURE
LES FOR NOZZLE 2 ($\dot{W}_s/\dot{W}_t = 0.16$)

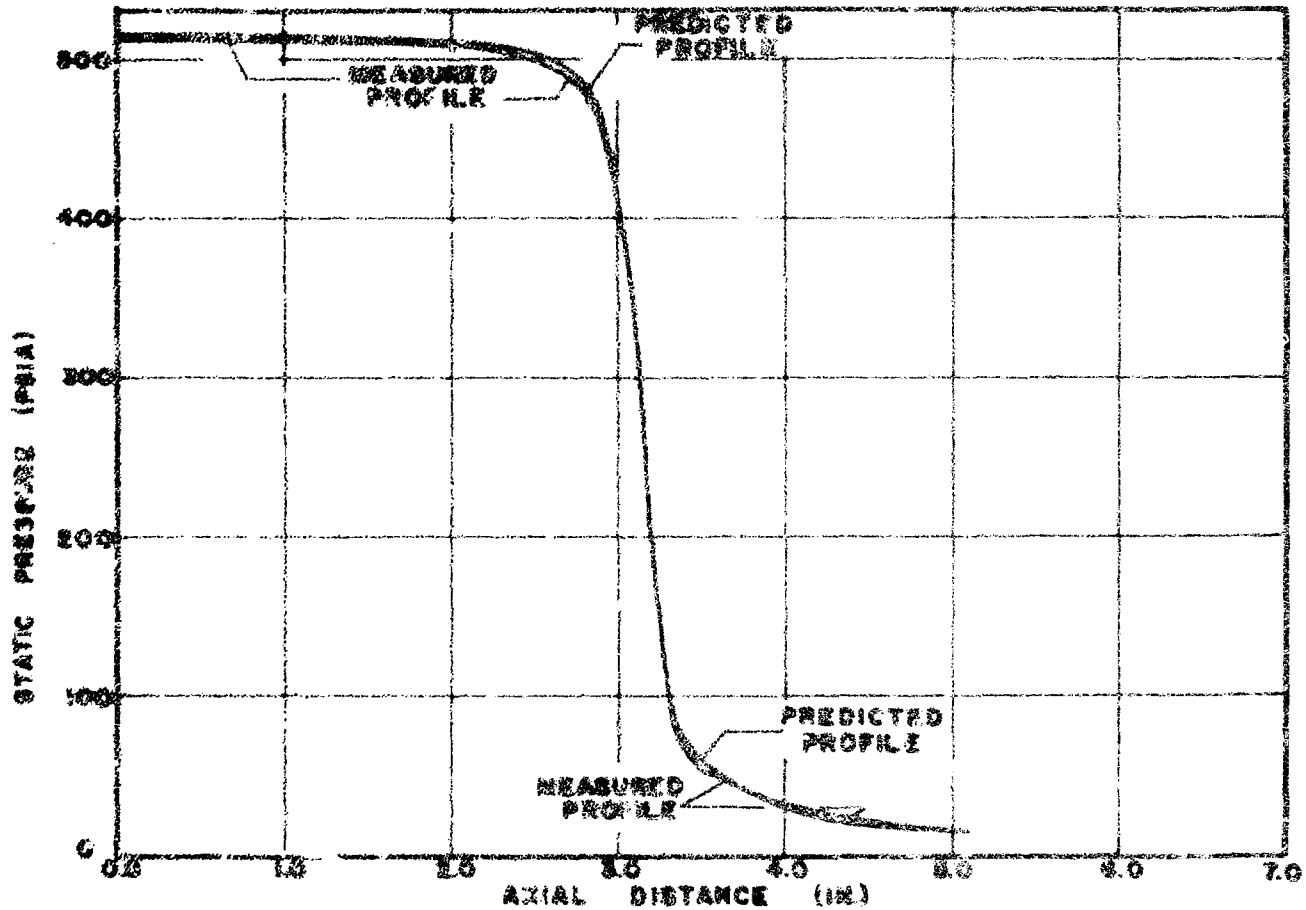

FIG. 14 PREDICTED AND MEASURED STATIC PRESSURE PROFILES FOR NOZZLE II ($M_s/M_\infty = 0.10$)

4-2 Flow Rates

A comparison of the predicted and measured flow rates is shown in Table 4.

Table 4

Predicted and Measured Flow Rates

Nozzle	Mixture Ratio	Predicted Total Flow Rate (lb/sec)	Measured Total Flow Rate (lb/sec)	Percent Error
I	0.10	10.04	10.58	5.4
I	0.15	8.58	9.35	8.9
II	0.10	10.14	10.58	4.3

Table 4 indicates that the isothermal model predicts the flow rate more accurately at the lower mixture ratios. At the higher mixture ratios there is less water and more air and therefore, less heat available for a larger amount of air than at the lower mixture ratios. This increase in inaccuracy of the isothermal model at the higher mixture ratios is also indicated by comparing Figures 12 and 13. The measured and predicted pressure profiles in the diverging portion of Nozzle I match more closely when the mixture ratio is 0.10 than when it is 0.15.

4-3 Thrust

The effective nozzle exit velocity is defined as follows:

$$V_N = F_g/\dot{W}_L + \dot{W}_G = F_g/\dot{W}_T = \text{Thrust/Total Flow Rate} \qquad (22)$$

and the equation for thrust (F) is given by,

$$F = (1/g)\,(\dot{W}_L V_{Le} + \dot{W}_G V_{Ge}) + (p_e - p_a)A_e \qquad (23)$$

where

V_{Ge} = gas exit velocity

V_{Le} = liquid exit velocity

p_e = nozzle exit pressure

p_a = ambient pressure

A_e = nozzle exit area

The last term of Equation 23 can be dropped since $p_e = p_a$ in both experimental and theoretical cases. The predicted and measured values of the effective nozzle exit velocity are presented in Table 5.

Table 5

Predicted and Measured Values of the Effective Nozzle Exit Velocity

Nozzle	Mixture Ratio	Thrust (lb)	Predicted Velocity(ft/sec)	Measured Velocity(ft/sec)	Percent Error
I	0.10	182.4	699	556	25.7
I	0.15	183.3	778	631	23.3
II	0.10	194.9	620	600	3.3

From Table 5 it is seen that the effective nozzle exit velocity calculated with the isothermal, frictionless model was far in error for Nozzle I. The calculation for Nozzle II however, was quite accurate. Nozzle I had a diverging angle of 7° and an overall length of 8.85 in. and Nozzle II had a diverging angle of 21° and an overall length of 5.1 in. The results presented in Table 5 indicate that friction plays

a dominate roll in the determination of the gas and liquid velocities when long nozzles are being investigated. Friction between the phases and between the mixture and the nozzle boundaries was neglected in this analysis. Non-ideal thermal equilibrium also causes a reduction in thrust. (2)

5 CONCLUSIONS

The use of the frictionless, isothermal model appears to be limited to those type nozzles suited for jet pump operation. These nozzles are short to conserve weight, and operate with low mixture ratios in order that as much liquid be pumped as possible with a corresponding low gas consumption.

Two modifications should be made to the isothermal model in order to widen the range of its usefulness; (1) consideration should be given to the heat transfer that occurs between the liquid and the gas, and (2) the effects of wall friction should be included.

5-1 Heat Transfer Between Phases

An analysis which takes into account the heat transfer between the liquid and the gas would employ the following equations and relationships in addition to those employed in the isothermal model.

1. Energy equation for mixture

$$\dot{W}_G \left[C_p dT_G + V_G \left(dV_G / Jg \right) \right] + \dot{W}_L \left[dh_L + V_L \left(dV_L / Jg \right) \right] = 0$$

2. $T_L = f(h_L)$

3. Heat Balance on the Droplet

$$dq_d/dt = -h_c A_d \Delta T = \rho_d \forall_d \, dh_d/dt$$

$$= \rho_d \forall_d V_d \, dh_d/dX$$

4. Experimental plot of Nusselt number vs. Reynolds number for spherical droplets (8).

where

V_d = droplet volume

A_d = droplet surface area

h_c = convective heat transfer coefficient

h_d = enthalpy of the droplet

q_d = convective heat transfer rate from the droplet

ΔT = temperature difference between the gas and the liquid

ρ_d = droplet density

Equation B-5, which is derived in Appendix B, shows the effect of a temperature drop of the gas on the gas velocity for the adiabatic model.

$$dV_{G\ \substack{\text{adiabatic}\\\text{model}}} = dV_{G\ \substack{\text{isothermal}\\\text{model}}} + \bar{V}_G(dT_G/\bar{T}_G) \qquad (B\text{-}5)$$

dT_G is negative and therefore dV_G is less for a given increment when employing the adiabatic model than when employing the isothermal model. A lower exit gas velocity results when considering the flow to be adiabatic which in turn reduces the thrust that can be obtained from the nozzle.

5-2 Friction Coefficient

It appears that a friction coefficient must be experimentally determined for the type of two-phase flow discussed herein. There is friction between the gas and liquid and between the mixture and the nozzle boundaries. For each different gas and/or liquid used, the influence of friction would be different. A theoretical determination of the friction coefficient appears to be improbable.

5-3 Recommendations

The analysis presented herein should be programmed for solution on a faster digital computer. If the heat transfer between the liquid and

the gas is to be considered it would be imperative that a faster computer be utilized. To determine the inlet conditions to seven significant figures for one nozzle and mixture ratio, approximately sixty hours of computer time were necessary when employing the RPC 4000. The solution would take a considerable amount of time even if a faster computer were utilized. Another method of numerical solution of the equations should therefore be investigated.

BIBLIOGRAPHY

BIBLIOGRAPHY

1. Elliott, D.G., Theoretical and Experimental Investigation of a Gas-Driven Jet Pump for Rocket Engines, Ph.D. Thesis, Purdue University, Lafayette, Indiana, 1959. (Classified) (The declassified portions of this reference as employed herein appear Liquid Rockets and Propellants, Progress in Astronautics and Rocketry, Vol. 2, Academic Press, New York, 1960.)

2. Crabtree, D. L., Investigation of the Influence of the Design Parameters on the Flow Characteristics of the Drive Nozzle of a Gas-Driven Jet Pump, M.S.M.E. Thesis, Purdue University, Lafayette, Indiana, 1961.

3. Isshiki, Naotsu Theoretical and Experimental Study on Atomization of (a) Liquid Drop in (a) High Speed Gas Stream, Transportation Technical Research Institute Report 55, Tokyo, Japan.

4. Richard, L. P. The Effect of an Initially Large Internal Temperature Difference, and Condensibility of the Gas on the Exit Velocity for Two-Phase Flow of a Liquid and a Gas in a Nozzle, M.S.M.E. Thesis, Purdue University, Lafayette, Indiana, 1959.

5. Schlichting, H., Boundary Layer Theory, McGraw-Hill Book Company, New York, 1960.

6. Rabin, E., Schallenmuller, A. R., Lawhead, R. B., Displacement and Shattering of Propellant Droplets, Final Summary Report, Rocketdyne, A Division of North American Aviation, Inc., March, 1960.

7. Ingebo, R. D., Drag Coefficients for Droplets and Solid Spheres in Clouds Accelerating in Airstreams, TN 3762, National Advisory Committee for Aeronautics, Washington, D. C., September 1956.

8. Kreith, F., Principles of Heat Transfer, International Textbook Company, Scranton, Pennsylvania, 1958.

9. Zucrow, M. J., Aircraft and Missle Propulsion, Vol. 1, John Wiley and Sons, New York, 1958.

Tangren, R. F., Dodge, C. H., and Seifert, H. S., Compressibility Effects in Two-Phase Flow, Journal of Applied Physics, Vol. 20, No. 7, July 1949.

11. Gilbert, M., Davis, L., and Altman, D., Velocity Lag of Particles in Linearly Accelerated Combustion Gases, Progress Report No. 20194, Jet Propulsion Laboratory, Pasadena, California, May 1953.

12. Seifert, H. S., Altman, D., A Comparison of Adiabatic and Isothermal Expansion Processes in Rocket Nozzles, A.R.S. Journal, Vol. 22, No. 3, May-June, 1952.

APPENDICES

APPENDIX A

NOMENCLATURE

a_d = acceleration of droplet, ft/sec^2

A_d = projected area of droplet, in.^{2}

A_e = nozzle exit area, in.^{2}

A_G = flow area of gas, in.^{2}

A_L = flow area of liquid, in.^{2}

A_S = one-dimensional surface area of diverging nozzle, in.^{2}

A_T = total flow area, in.^{2}

C_D = drag coefficient

C_L = specific heat of water, B/lb-$^\circ$R

C_p = specific heat of air at constant pressure, B/lb-$^\circ$R

F = thrust, lb

F_D = drag force, lb

F_p = pressure force, lb

F_x = force in X-direction, lb

g = gravity constant, 32.174 ft/sec^2

J = mechanical equivalent of heat, 778 ft-lb/B

m_d = mass of droplet, slugs

$\dot{m}_G$ = mass flow rate of gas, slugs/sec

$\dot{m}_L$ = mass flow rate of liquid, slugs/sec

N_R = Reynolds number

N_{We} = Weber number

p = pressure, psia

P = pressure, psia

p_a = ambient pressure, psia

p_e = nozzle exit pressure, psia

P_N = nozzle inlet pressure, psia

P_x = X-component of pressure acting on droplet, psia

$\bar{R}$ = Universal gas constant, ft-lb/ mole-R

R = gas constant for air, 53.3 ft-lb/lb-R

r = droplet radius, in.

T_G = gas temperature, R

T_L = liquid temperature, R

T_N = inlet mixture temperature, R

V_G = gas velocity, ft/sec

V_L = liquid velocity, ft/sec

V_N = effective nozzle exit velocity, ft/sec

V_R = relative velocity between gas and liquid, ft/sec

W = molecular weight of gas

$\dot{W}_G$ = mass flow rate of gas, lb/sec

$\dot{W}_L$ = mass flow rate of liquid, lb/sec

$\dot{W}_T$ = total flow rate, lb/sec

X = distance along nozzle axis, in.

Z = any flow parameter

γ_L = specific weight of liquid, lb/ft^3

γ_G = specific weight of gas, lb/ft^3

μ = gas viscosity, slugs/ft-sec

ρ_L = density of liquid, slugs/

ρ_G = density of gas, slugs/ft^3

$\forall_d$ = droplet volume, in.^{3}

σ = surface tension of liquid, lb/ft

APPENDIX B

COMPARISON OF ADIABATIC AND ISOTHERMAL EQUATIONS

In order to compare the equations for the adiabatic and the isothermal models, all of the equations for both cases are left alike except for the equations for dV_G.

Rewriting equation 21

$$dV_{G\ \substack{\text{isothermal}\\ \text{model}}} = -\bar{V}_G\ (dA_G/\bar{A}_G) - \bar{V}_G\ (d\rho_G/\bar{\rho}_G) \qquad (21)$$

Writing the perfect gas law for the adiabatic model ($T_G \neq$ constant) and rearranging terms

$$\rho_G = p/gRT$$

Performing logarithmic differention,

$$d\rho_G/\rho_G = dp/p - dT_G/T_G \qquad (B\text{-}1)$$

Substituting equation (B-1) into equation (21)

$$dV_{G\ \substack{\text{adiabatic}\\ \text{model}}} = -\bar{V}_G(dA_G/\bar{A}_G) - \bar{V}_G(dp/\bar{p} - dT_G/\bar{T}_G) \qquad (B\text{-}2)$$

For isothermal flow $dT_G/T_G = 0$ and from equation (B-1)

$$d\rho_G/\rho_G = dp/p \qquad (B\text{-}3)$$

Substituting equation B-3 into equation 21

$$dV_{G\ \substack{\text{isothermal}\\ \text{model}}} = -\bar{V}_G(dA_G/\bar{A}_G) - \bar{V}_G\ (dp/\bar{p}) \qquad (B\text{-}4)$$

Substituting equation B-4 into equation B-2

$$dV_{G\ \text{adiabatic model}} = dV_{G\ \text{isothermal model}} + \bar{V}_G(dT_G/\bar{T}_G) \qquad (B\text{-}5)$$

"Distribution of this report has been made in accordance with the Joint Army-Navy-Air Force Liquid Propellant Mailing List of March 1962."